Spectral and timing evolution of GRO J1655-40 during its outburst of 2005

D. Debnath[1,2, *], Sandip K. Chakrabarti[3,1,2], A. Nandi[1,4] and S. Mandal[1]

[1] *Indian Centre for Space Physics, Chalantika 43, Garia Station Rd., Kolkata, 700084, India*

[2] *Visitor, Abdus Salam International Centre for Theoretical Physics, Strada Costiera, 34100, Trieste*

[3] *S. N. Bose National Center for Basic Sciences, JD-Block, Salt Lake, Kolkata, 700098, India*

[4] *On deputation from ISRO HQ, New BEL Road, Bangalore, 560231, India*

Abstract. In a recent outburst which lasted for 260 days, the black hole candidate GRO J1655-40 exhibited a behaviour similar to its last outburst observed almost eight years ago. We analyze a total of 150 observational spells in 122 days of data spreaded over the entire outburst phase of Feb. 2005 to Oct. 2005. From our study, a comprehensive understanding of the detailed behaviour of this black hole candidate has emerged. Based on the degree of importance of the black body and the power-law components we divide the entire episode in four spectral states, namely, *hard, soft, very soft* and *intermediate*. Quasi-Periodic oscillations (QPOs) were found in two out of these four states, namely, in the hard and the intermediate states. In the hard state, at the rising phase of the outburst, QPO frequency ranged from 0.034 - 17.78Hz and the spectra was fitted by a disk black body, power-law and iron emission line at 6.2 - 6.5 keV. In the intermediate state, QPOs vary from 13.17Hz to 19.04Hz and the QPO frequency modulation in this state was not significant. The spectra in this state are well fitted by the disk black body and the power-law components. In the hard state of the declining phase of the outburst, we found QPOs of decreasing frequency from 13.14 Hz to 0.034 Hz. The spectra of this state were fitted by a disk black body and power-law components, but in the initial few days a cooler Comptonized component was required for a better fit. In the soft/very soft states, the spectral states are mostly dominated by the strong disk black body component.

Keywords : stars: Individual (GRO J1655-40) — X-ray sources – Spectrum –Radiation hydrodynamics

*e-mail: dipak@csp.res.in, chakraba@bose.res.in, anuj@csp.res.in, samir@csp.res.in

1.   Introduction

The Galactic black hole candidates are the most fascinating objects to study in X-rays, as these sources undergo peculiar timing and spectral changes during their transient as well as the persistent phases. The soft X-ray transient GRO J1655-40 was first observed by BATSE on board CGRO on 27th July 1994 (Zhang et al. 1994). This source was extensively observed with RXTE during 1996 and 1997 and it showed a very complex timing and spectral behaviour and the source was X-ray active at least for 16 months.

GRO J1655-40, an enigmatic Low Mass X-ray Binary (LMXB) system is located at $(l, b) = (344.98°, 2.45°)$ (Bailyn et al. 1995) with R.A.=$16^h 54^m 00^s$ and Dec.=$-39°50^m 45^s$. Its mass (M = 7.02 ± 0.22 $M_\odot$; Orosz & Bailyn 1997) distance (D = 3.2 ± 0.2 kpc; Hjellming & Rupen 1995), and inclination angle ($\theta = 69.5° \pm 0.1°$; Orosz & Bailyn 1997) are well determined. The mass of its companion star is = 2.3 $M_\odot$ (Bailyn et al. 1995). GRO J1655-40 may also have shown signatures of the ejection of the superluminal radio jet (Tingay et al. 1995; Hjellming & Rupen 1995). Recent VLT-UVES spectroscopic observations suggest that the distance to the source is ≤ 1.7 kpc (Foellmi et al., 2006) with a secondary star of spectral type of F6IV, making it one of the closest known black hole candidates. The maximum speed of the jet was found to be $\sim 0.37c$.

The first observed outburst showed a double peaked profile in the ASM light curve and it is quite different from other black hole candidates. The first peak in May, 1996, the source showed a strong flaring activity with non-thermal emission, whereas during the second peak in August, 1997, the source spectrum was softer and thermal, except near the end of the outburst when its spectrum was hard (Sobczak et al. 1999). At least three distinct spectral states, namely, very high state, high/soft state and low/hard state (Sobczak et al. 1999) have been reported. The luminosity variation of the outburst was of fast rise and exponential decay (Chen et al. 1997). Investigation of X-ray timing properties of GRO J1655-40 during the 1996-97 outburst revealed QPOs varying from 0.1 Hz to 300 Hz (Remillard et al. 1999). Two very important discoveries were found there: one is the superluminal radio jet (Tingay et al. 1995; Hjellming & Rupen 1995) and the other is the existence of very high QPO frequencies (300 & 450 Hz) (Remillard et al. 1999; Strohmayer 2001).

After remaining 'dormant' for almost eight years, GRO J1655-40 showed a renewed X-ray activity in late February 2005 (Markwardt & Swank 2005, Chakrabarti et al. 2005; Shaposhnikov et al. 2007). The source remained active in X-rays for the next 260 days and during this period, it was extensively observed with the RXTE Satellite. In the present paper, we analyze the archival data of RXTE instruments (ASM and PCA) and present the results for both the timing and the spectral properties of GRO J1655-40 during this outburst phase. In the entire outburst phase, we identified four spectral states characterized by the presence or absence of a soft black body component at low energy and the power-law component at higher energies above ~ 10 keV. Since there are confusions in the literature regarding the nomenclature vis-á-vis the properties, we define them here

at appropriate places. The four identified states are termed as the hard, soft/very-soft and intermediate states. During the total outburst we observed the transitions in this sequence: hard → soft/very soft → intermediate → hard. In each of these spectral states, we carried out the timing analysis and find QPO frequencies. The Power Density Spectra (PDS) are quite different in different spectral states and sometimes the nature of the PDS is highly correlated with the spectral features. The justification of these four classifications will be presented later. In previous communications (Chakrabarti et al. 2005; Chakrabarti et al. 2008) the evolution of the QPO frequencies with time was shown in the initial and final outburst stages. The rapid variation in QPO frequencies was explained by using an oscillating and propagating shock.

Prior to our present analysis, Shaposnikov et al. (2007) carried out a multi-wavelength study for the early stage (beginning with 21st of February, 2005) of the outburst of GRO J1655-40 for a total of 25 days of data using instruments like RXTE & INTEGRAL for X-rays, VLA for radio study and ROSTE & SMARTS for optical region. On the basis of their multi-wavelength campaign they classified the spectral states of the observed period in four spectral states, namely, low-hard, hard intermediate, soft intermediate, high-soft. After correlating X-ray and radio fluxes they concluded that the physical origins of the radio emission and the X-ray emission are not the same. The evidence of a closer coupling between the power-law component and QPO as also observed by Vignarca et al. (2003) is totally consistent with the shock propagation model of Chakrabarti et al. (2005, 2008) as the shock does not propagate in the *disk* as they mentioned, but through the sub-Keplerian flow which surrounds the disk (e.g., Chakrabarti & Titarchuk 1995).

Our study, on the other hand, covers 122 days of the observational data spreading over the full period of the outburst. On the basis of the results of RXTE data, we classified the total outburst in a slightly different way with four distinct spectral states. Furthermore, we thoroughly studied the QPO behaviour. We got QPOs in a total of 67 observations out of a total of 150 observations. We also studied the photon count variation in different energy bands for different spectral states via hardness and softness intensity diagrams. We identify the energy band in which QPOs are predominantly seen. We show spectral components and their flux variations. We claim that two components of the flow, namely, the Keplerian and the sub-Keplerian (halo) are necessary to explain the mass accretion dynamics. We theoretically estimate the disk and the halo rates from spectral fits of several observations.

In passing, we may mention that some other workers reported analysis of the outburst using Swift (Brocksopp et al. 2006) and XMM-Newton & INTEGRAL (Trigo et al. 2007). The Suzaku data of the late phase of the outburst has been analyzed by Takahashi et al. (2008) who showed that two different Comptonizing electron clouds are required to explain the high energy spectra in the low/hard state. This agrees with our findings also (Chakrabarti et al. 2008). This will be illustrated in more detail in the present paper as well.
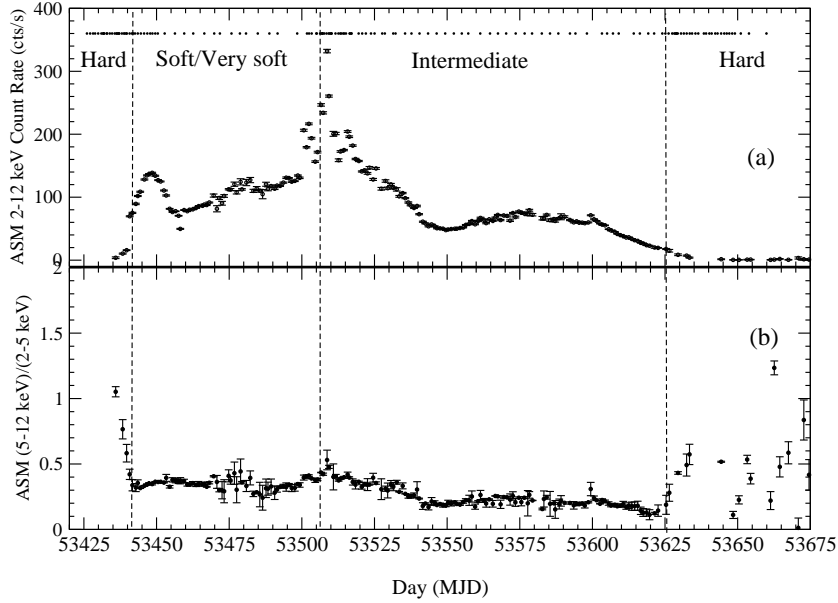
Figure 1. (a) 2-12 keV ASM light curve and (b) hardness ratio (5-12 keV vs. 2-5 keV count ratio) as a function of the MJD of the event. The vertical dashed lines indicate the transition of states.

The paper is organized in the following way: In the next Section, we analyze the data and present the results of our analysis. This includes the timing analysis of ASM and PCA data and spectral analysis of PCA data. In Section 3, we present the brief interpretation of the overall results. Finally, in Section 4, we make concluding remarks.

2.   Observation and data analysis

2.1   Analysis of ASM and Light Curves

We analyze publicly available observational data from the RXTE instruments of the 2005 outburst. Here, we present the results from the All Sky Monitor (ASM) and Proportional Counter Array (PCA) covering the entire eight months of the outburst of GRO J1655-40. Our analysis covers from the 25th of February, 2005 (MJD = 53426) to 16th of October, 2005 (MJD = 53659). The ASM data has four energy bands corresponding to $2 - 3$ keV, $3 - 5$ keV, $5 - 12$ keV and $2 - 12$ keV. PCA contains five proportional counter units (PCUs 0-4). We used only PCU 2 data for both the timing and spectral analysis due to its reliability and it is on for 100% of the goodtime. Data reduction and analysis were carried out with the FTOOLS version of HEADAS-6.1.1 software and XSPEC version 12.3.0.
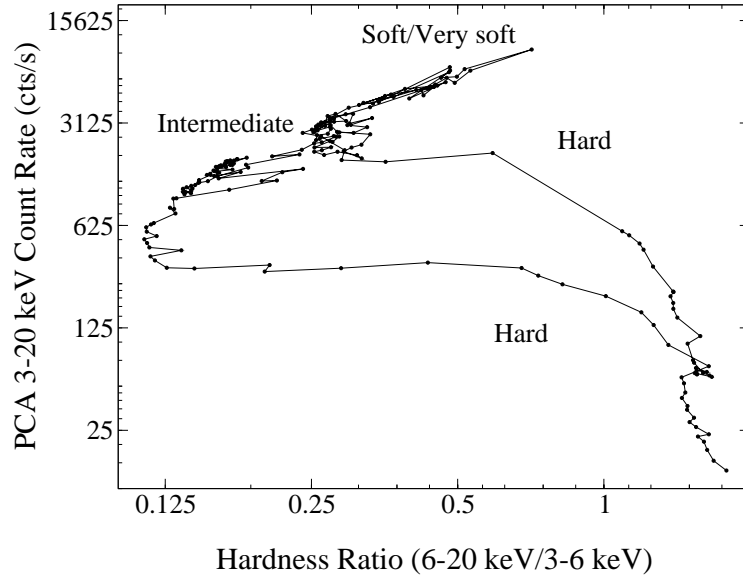
Figure 2. The Hardness Intensity Diagram (HID) observed with RXTE/PCA. Count rates are in 3-20 keV energy band and hardness ratio is defined as the ratio of count rates in the 6-20 keV and 3-6 keV bands.

We have extracted and analyzed the ASM (Levine et al. 1998) data of different energy bands for the entire observation. In Figs 1(a-b), the total 2-12 keV ASM light curve (counts/sec) and the ASM hardness ratio (ratio of the photon count rates in 5-12 keV and 2-5 keV bands) are plotted. The origin of the time axis is MJD 53420 (19th February, 2005), which is six days before the initial rise of the X-ray intensity. The hardness ratio variation distinctly reflects the state transitions. The hard to soft transition takes place on the 13th of March, 2005 (MJD = 53442), the soft to intermediate transition on the 16th of May, 2005 (MJD = 53506), and the intermediate to hard transition takes place on the 12th of September, 2005 (MJD = 53625). These are marked on the plot. However, the local changes in the spectral features of different states are not evident from this plot. This leads us to conduct a robust spectral analysis using the PCA data and the results are presented below.

The RXTE archival data from February 25th, 2005 (MJD = 53426) to October 16th, 2005 (MJD = 53659) were extracted and analyzed from the Proportional Counter Array (PCA; Jahoda et al., 1996). We extract light curves (LC), PDS (with 0.01s binning of PCA data from $3 - 25$ keV) and the energy spectra from the good and the best-calibrated detector units *i.e.*, PCU2, for the PCA. We use the latest FTOOLS software package. For the timing analysis (LC & PDS) from February 25th, 2005 (MJD = 53426) to March, 11th, 2005 (MJD = 53440), we use the Science Data of the Event mode

($E\_125us\_64M\_0\_1s$, FS4f*gz) and for the rest of the observed dates we use the Science Data of the Binned mode ($B\_8ms\_16A\_0\_35\_H$, FS37*.gz) and of the Event mode ($E\_62us\_32M\_36\_1s$, FS3b*.gz). To extract the light curves from the Event mode data files, we use the "sefilter" task and for the Binned mode data files, we use the "saextrct" task. For the spectral analysis, we use Standard2 Science Data of PCA (FS4a*.gz). The "pcabackest" task was used for the PCA background estimation purpose. Here we used bright source epoch 5 background model file for calculating PCA background. We also incorporated *pca_saa_history* file for taking care of saa data. To generate the response files, we use the "pcarsp" task. For the rebinning of the pha files created by the "saextrct" task, we use the "rbnpha" task.

In Fig. 2 we plotted the PCA 3-20 keV count rate of the 2005 outburst against X-ray color (ASM count ratio between 6-20 keV and 3-6 keV energy bands). It is evident that the pre and post-outburst phases tend to appear and disappear from the low count region having harder spectrum. In GRO J1655-40 outburst, the transition occurs from the spectral states *hard → soft (very soft) → intermediate → hard*. It is observed that the rapid changes in the hardness ratio occurs only in the hard states, whereas in the soft and intermediate states the hardness ratio changes very slowly. Both rising and falling arms of the diagram corresponds to the hard state. In both the cases, we found the presence of QPOs. The possible physical origin will be discussed in Section 2.

In the first phase of the hard state from the 25th of February, 2005 (MJD = 53426) to the 12th of March, 2005 (MJD = 53441), we found QPOs from 34 mHz to 17.78 Hz. The observed QPO frequencies were found to be increased monotonically with time (day) from 0.082 Hz to 17.78 Hz (on the first day another QPO at 34 mHz was also seen.) The soft state starts from the 13th of March, 2005 (MJD = 53442) and continued till 15th of May, 2005 (MJD = 53505). In this region no QPO was observed. The intermediate state is seen from the 16th of May, 2005 (MJD = 53506) to 11th of September, 2005 (MJD = 53624). Interestingly, we found QPOs only for 8 days, from 16th of May, 2005 (MJD = 53506) to 20th of May, 2005 (MJD = 53510) and from 25th of May, 2005 (MJD = 53515) to 27th of May, 2005 (MJD = 53517). In between, for four days we observed no signature of QPOs. The QPO frequencies varied from 13.17 Hz to 19.04 Hz. In the PDS, we also found one broad QPO bump at frequencies near 7 Hz. The final hard state observed is from the 12th of September, 2005 (MJD = 53625) to 16th of October, 2005 (MJD = 53659). The QPOs of 0.023 Hz to 20.20 Hz QPOs were observed in this state. If we follow one of the QPO frequencies, we find it to decrease monotonically from 13.14 Hz to 0.034 Hz within 20 days.

2.2   Timing Analysis

We carried out the detailed timing analysis of the total 122 days data of 150 observational IDs. We used the PCU2 data from the Event mode ($E\_125us\_64M\_0\_1s$) and Science Array mode ($B\_8ms\_16A\_0\_35\_H$) data for the timing analysis. Our timing analysis is
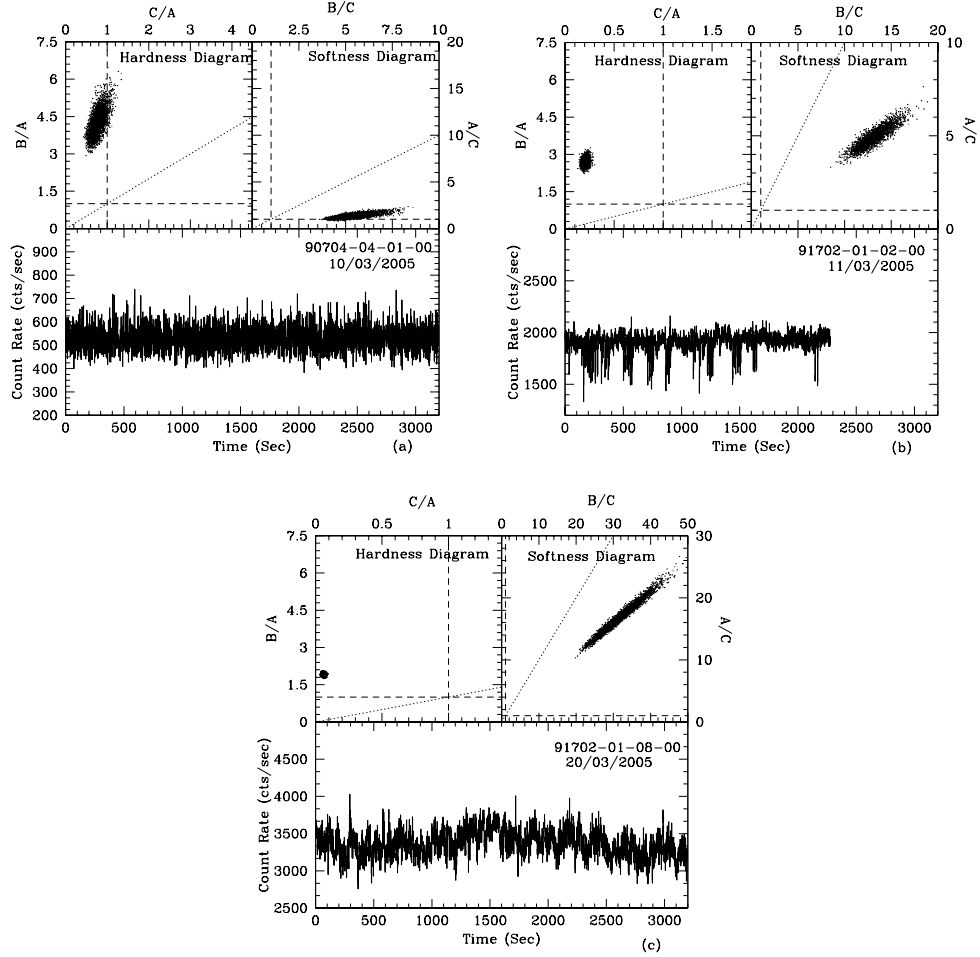
Figure 3. (**a-b**) In the lower panel, 2 - 15 keV (0-35 Channels) PCA light curve and in the upper panel the hardness and softness diagrams are plotted. Both the figures are of hard state observed on 10th of March and 11th of March, 2005. Drastic changes in timing features are observed in these two consecutive days, see text for details. In hardness diagrams, the dashed horizontal ($B = A$), vertical ($C = A$) and the dotted line ($B = C$) are for reference purpose. In softness diagram they represent $C = A$, $B = C$ and $A = B$ respectively. (**c**) Same as in Figs 3(a-b), except that the observation is of 20th March, 2005 when the source was in a soft state.

mainly to study the light curves with hardness and softness variation and the PDS of each data. Out of these observations, we find QPOs in a total of 67 observations made in 43 days. A summary of the results are presented in Table 1. Here, we list the observing date and time and the PCA count rates (photon counts/sec) for PCU2 in 3 different energy
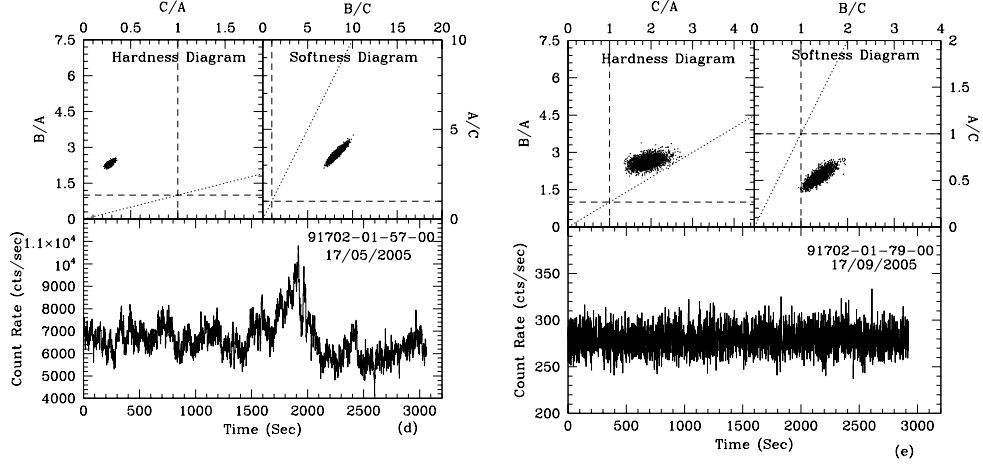
Figure 3 (d-e): Same as in Figs. 3(a-b) except for (d) the intermediate state (17th of May, 2005) and (e) the hard state of the decline phase (17th of Sept., 2005).

bands, E1: $2-3.5$ keV ($0-7$ channels), E2: $3.5-10.5$ keV ($8-24$ channels) and E3: $10.5-60$ keV ($25-138$ channels). We also list two hardness ratios (E2/E1 and E2/E3) and the observed QPO frequencies (in Hz).

2.2.1 Light curves with hardness and softness diagrams

We extracted 2 - 15 keV (0-35 Channels) PCA light curve with a time bin of 1 sec. To have the qualitative analysis of photon count variations in different energy bands, we plotted both the hardness and softness ratio variations. To plot the hardness and the softness ratios, we extracted light curves for three energy bands: $A : 0-8$ channels ($2-4$ keV), $B : 9-35$ channels ($4-15$ keV) and $C : 36-138$ channels ($15-60$ keV). A hardness diagram is the plot between C/A vs. B/A while the softness diagram is the plot between B/C vs. A/C. Our motivation of splitting the energies in this way stems from the fact that the Keplerian disk primarily emits at a low energy ($\lesssim 4$ kev) for the mass of the black hole we are interested in. Thus, A will be emitted mostly from the Keplerian component. The component B would be emitted from the region where the moderate thermal Comptonization of the Keplerian photons take place. The component C would be emitted from the region which is definitely depleted or enhanced during state transitions as it represents the higher energy side of the pivotal energy [~ 15 keV] in the spectrum. Thus, these diagrams are not directly connected to the spectral states – rather, they are connected to the geometry, i.e., the number of soft photons produced by the Keplerian disk ($\sim A$) and the seed photons intercepted by the 'Compton cloud' [$\sim (B+C)$] and the number of scatterings they undergo ($\sim B$ or $\sim C$).

Table 1. PCA Count rates, Hardness ratios and QPOs.

Obs. (1)	UT Date (2)	MJD Start (3)	MJD Stop (4)	PCA 2-3.5 keV (5)	PCA 3.5-10.5 keV (6)	PCA 10.5-60 keV (7)	$HR5^a$ (8)	$HR6^b$ (9)	QPO Frequency (10)
1	25/02/05	53426.0400	53426.0806	4	30	29	7.341	1.026	0.082
2	26/02/05	53427.1546	53427.1939	5	37	34	7.234	1.088	0.034, 0.106
3	27/02/05	53428.1380	53428.1786	5	39	35	7.350	1.118	0.116
4	27/02/05	53428.8594	53428.8994	5	40	35	7.381	1.161	0.051, 0.122
5	28/02/05	53429.9080	53429.9480	5	40	35	7.341	1.146	0.051, 0.121
6	02/03/05	53431.0224	53431.0626	5	37	34	7.328	1.097	0.036, 0.109
7	02/03/05	53431.6122	53431.6355	5	38	34	7.349	1.121	0.045, 0.129
8	02/03/05	53431.7435	53431.7758	4	35	33	8.288	1.068	0.050, 0.117
9	02/03/05	53431.8096	53431.8320	4	37	33	8.363	1.104	0.122
10	02/03/05	53431.9398	53431.9800	5	38	34	7.561	1.116	0.121
11	03/03/05	53432.7930	53432.8320	6	45	37	7.425	1.195	0.163
12	04/03/05	53433.0017	53433.0286	6	46	39	7.191	1.174	0.160
13	05/03/05	53433.9050	53434.0119	8	61	47	7.198	1.312	0.247
14	05/03/05	53434.6935	53434.7230	8	70	52	8.324	1.334	0.116, 0.317
15	06/03/05	53435.6115	53435.6355	13	94	63	7.192	1.499	0.383
16	07/03/05	53436.1594	53436.1751	15	108	69	6.919	1.557	0.417
17	07/03/05	53436.3976	53436.4084	17	119	75	6.981	1.577	0.149, 0.487
18	07/03/05	53436.7254	53436.7654	18	131	80	6.943	1.628	0.125, 0.487
19	08/03/05	53437.0715	53437.0932	19	142	87	7.165	1.638	0.119, 0.513
20	08/03/05	53437.1415	53437.1584	20	143	87	7.108	1.646	0.033, 0.517
21	09/03/05	53438.0539	53438.0765	32	215	116	6.588	1.858	0.886
22	09/03/05	53438.7574	53438.7973	44	285	140	6.428	2.026	1.349
23	10/03/05	53439.1067	53439.1251	49	315	149	6.346	2.102	0.089, 1.528
24	10/03/05	53439.6096	53439.6362	58	361	162	6.133	2.229	2.035
25	10/03/05	53439.7400	53439.7806	65	386	167	5.930	2.312	2.313, 4.620

[a] Ratio of 3.5-10.5 keV and 2-3.5 keV PCA count rates.
[b] Ratio of 3.5-10.5 keV and 10.5-60 keV PCA count rates.

Table 1. Continued.

Obs. (1)	UT Date (2)	MJD Start (3)	MJD Stop (4)	PCA 2-3.5 keV (5)	PCA 3.5-10.5 keV (6)	PCA 10.5-60 keV (7)	$HR5^a$ (8)	$HR6^b$ (9)	QPO Frequency (10)
26	11/03/05	53440.7357	53440.7640	332	1415	283	4.260	4.989	3.262, 6.546
27	12/03/05	53441.5109	53441.5306	371	1230	123	3.312	9.923	14.54, 17.78
28	12/03/05	53441.9852	53442.0091	406	1268	92	3.123	13.782	...
29	13/03/05	53442.5865	53442.5994	459	1498	103	3.263	14.543	...
30	14/03/05	53443.5431	53443.5827	570	1892	89	3.319	21.258	...
31	15/03/05	53444.5891	53444.8102	600	2030	61	3.383	33.278	...
32	16/03/05	53445.7141	53445.8313	677	2436	95	3.598	25.642	...
33	17/03/05	53446.8241	53446.8539	673	2462	105	3.658	23.447	...
34	18/03/05	53447.8176	53447.8570	747	2787	83	3.730	33.578	...
35	19/03/05	53448.5876	53448.7730	730	2699	69	3.697	39.115	...
36	20/03/05	53449.5726	53449.6852	658	2468	59	3.750	41.830	...
37	21/03/05	53450.4246	53450.6809	651	2415	54	3.709	44.722	...
38	23/03/05	53452.7930	53452.8352	551	2118	58	3.843	36.517	...
39	27/03/05	53456.3239	53456.4998	398	1567	45	3.937	34.822	...
40	30/03/05	53459.5389	53459.5770	404	1552	43	3.841	36.093	...
41	02/04/05	53462.6287	53462.6581	431	1579	39	3.663	40.487	...
42	06/04/05	53466.4356	53466.4528	492	1821	48	3.701	37.937	...
43	09/04/05	53469.8446	53469.8820	522	1981	50	3.795	39.620	...
44	11/04/05	53471.8050	53471.9174	513	1844	42	3.594	43.904	...
45	15/04/05	53475.7913	53475.8630	587	2225	54	3.790	41.203	...
46	18/04/05	53478.6883	53478.7235	582	2088	46	3.587	45.391	...
47	20/04/05	53480.7857	53480.8907	626	2318	54	3.702	42.925	...
48	24/04/05	53484.8274	53484.9526	610	2168	47	3.554	46.127	...
49	28/04/05	53488.8376	53488.8865	673	2545	61	3.781	41.721	...
50	01/04/05	53491.6635	53491.7706	632	2292	50	3.626	45.840	...

^{a}Ratio of 3.5-10.5 keV and 2-3.5 keV PCA count rates.
^{b}Ratio of 3.5-10.5 keV and 10.5-60 keV PCA count rates.

Table 1. Continued.

Obs. (1)	UT Date (2)	MJD Start (3)	MJD Stop (4)	PCA 2-3.5 keV (5)	PCA 3.5-10.5 keV (6)	PCA 10.5-60 keV (7)	$HR5^a$ (8)	$HR6^b$ (9)	QPO Frequency (10)
51	08/05/05	53498.4152	53498.6526	694	2615	70	3.768	37.357	...
52	11/05/05	53501.7698	53501.7991	866	3507	250	4.049	14.028	...
53	12/05/05	53502.4883	53502.5206	1266	5220	517	4.123	10.096	...
54	13/05/05	53503.3948	53503.4491	914	3602	219	3.940	16.447	...
55	14/05/05	53504.9885	53505.0170	884	3542	171	4.006	20.713	...
56	15/05/05	53505.1231	53505.1418	851	3353	163	3.940	20.570	...
57	16/05/05	53506.2788	53506.2994	1202	5081	562	4.225	9.031	18.19
58	16/05/05	53506.9530	53506.9654	1370	5642	555	4.116	10.151	19.04
59	17/05/05	53507.0211	53507.0382	1303	5350	534	4.105	10.014	18.30
60	17/05/05	53507.0865	53507.1098	1166	4801	440	4.117	10.911	18.21
61	17/05/05	53507.1959	53507.2404	1164	4792	462	4.115	10.365	18.94
62	17/05/05	53507.7315	53507.7445	1294	5447	611	4.209	8.903	18.65
63	18/05/05	53508.5072	53508.5528	1459	7160	1161	4.905	6.165	6.566, 18.30
64	19/05/05	53509.2280	53509.2744	1249	5310	627	4.248	8.469	17.41
65	19/05/05	53509.5587	53509.6021	1050	4407	471	4.194	9.351	18.19
66	20/05/05	53510.0315	53510.0452	1147	4794	463	4.177	10.346	13.17
67	20/05/05	53510.0996	53510.1271	962	3917	291	4.069	13.460	13.76
68	20/05/05	53510.2767	53510.3098	1029	4248	388	4.128	10.929	13.58
69	21/05/05	53511.5928	53511.6333	1002	4101	255	4.093	16.055	...
70	22/05/05	53512.5750	53512.6154	828	3212	119	3.877	26.973	...
71	23/05/05	53513.2291	53513.2771	911	3588	180	3.937	19.921	...
72	23/05/05	53513.5570	53513.5980	829	3282	147	3.959	22.326	...
73	24/05/05	53514.2272	53514.2612	856	3322	132	3.880	25.140	...
74	24/05/05	53514.6076	53514.6500	935	3771	207	4.033	18.217	...
75	25/05/05	53515.2040	53515.2452	1018	4185	394	4.109	10.595	16.13

[a] Ratio of 3.5-10.5 keV and 2-3.5 keV PCA count rates.
[b] Ratio of 3.5-10.5 keV and 10.5-60 keV PCA count rates.

Table 1. Continued.

Obs. (1)	UT Date (2)	MJD Start (3)	MJD Stop (4)	PCA 2-3.5 keV (5)	PCA 3.5-10.5 keV (6)	PCA 10.5-60 keV (7)	$HR5^a$ (8)	$HR6^b$ (9)	QPO Frequency (10)
76	26/05/05	53516.4476	53516.4765	897	3674	316	4.091	11.606	16.63
77	26/05/05	53516.5739	53516.6146	990	3977	326	4.015	12.194	16.89
78	27/05/05	53517.0383	53517.0806	1063	4306	402	4.047	10.704	16.75
79	27/05/05	53517.0989	53517.1223	1004	3970	312	3.953	12.710	...
80	29/05/05	53519.5456	53519.5609	873	3384	181	3.876	18.696	...
81	30/05/05	53520.7737	53520.8237	820	3058	116	3.729	26.362	...
82	01/06/05	53522.0243	53522.1276	721	2603	83	3.610	31.361	...
83	02/06/05	53523.7904	53523.8531	748	2744	115	3.668	23.860	...
84	04/06/05	53525.0356	53525.0761	758	2737	136	3.610	20.125	...
85	06/06/05	53527.6578	53527.7193	658	2345	123	3.563	19.065	...
86	07/06/05	53528.5739	53528.6111	709	2529	169	3.567	14.964	...
87	10/06/05	53531.4615	53531.4880	629	2178	151	3.462	14.423	...
88	11/06/05	53532.2446	53532.2604	584	1987	130	3.402	15.284	...
89	14/06/05	53535.5220	53535.5824	524	1710	90	3.263	19.000	...
90	16/06/05	53537.7478	53537.7887	487	1511	73	3.102	20.698	...
91	19/06/05	53540.5000	53540.6233	421	1176	40	2.793	29.400	...
92	22/06/05	53543.4491	53543.6206	345	893	27	2.588	33.074	...
93	25/06/05	53546.3970	53546.5185	323	806	22	2.495	36.636	...
94	28/06/05	53549.3456	53549.4698	296	733	22	2.476	33.318	...
95	01/07/05	53552.3067	53552.4770	301	747	20	2.481	37.350	...
96	04/07/05	53555.0476	53555.1130	314	789	19	2.512	41.526	...
97	06/07/05	53557.2754	53557.3193	328	842	22	2.567	38.272	...
98	10/07/05	53561.4059	53561.4485	367	1005	21	2.738	47.857	...
99	13/07/05	53564.7607	53564.7665	391	1078	23	2.757	46.869	...
100	16/07/05	53567.5052	53567.5485	404	1126	24	2.787	46.916	...

[a]Ratio of 3.5-10.5 keV and 2-3.5 keV PCA count rates.
[b]Ratio of 3.5-10.5 keV and 10.5-60 keV PCA count rates.

Table 1. Continued.

Obs. (1)	UT Date (2)	MJD Start (3)	MJD Stop (4)	PCA 2-3.5 keV (5)	PCA 3.5-10.5 keV (6)	PCA 10.5-60 keV (7)	$HR5^a$ (8)	$HR6^b$ (9)	QPO Frequency (10)
101	19/07/05	53570.3257	53570.3546	412	1160	25	2.815	46.400	...
102	22/07/05	53573.6024	53573.8011	439	1255	26	2.858	48.269	...
103	25/07/05	53576.6861	53576.7248	428	1230	27	2.873	45.555	...
104	28/07/05	53579.2404	53579.2644	441	1261	26	2.859	48.500	...
105	31/07/05	53582.5831	53582.6220	425	1198	26	2.818	46.076	...
106	03/08/05	53585.3994	53585.4935	416	1184	29	2.846	40.827	...
107	06/08/05	53588.2822	53588.2963	411	1145	22	2.785	52.045	...
108	10/08/05	53592.2800	53592.4054	391	1092	32	2.792	34.125	...
109	12/08/05	53594.1800	53594.2193	379	1039	27	2.741	38.481	...
110	16/08/05	53598.1106	53598.1511	352	940	28	2.670	33.571	...
111	21/08/05	53603.2907	53603.3369	331	895	47	2.703	19.042	...
112	23/08/05	53605.0552	53605.1170	304	769	35	2.529	21.971	...
113	25/08/05	53607.0900	53607.1296	281	662	21	2.355	31.523	...
114	27/08/05	53609.0546	53609.0970	248	567	22	2.286	25.772	...
115	01/09/05	53614.2289	53614.2715	192	407	18	2.119	22.611	...
116	03/09/05	53616.3294	53616.3728	167	354	19	2.119	18.6317...	
117	06/09/05	53619.2367	53619.2485	146	288	19	1.972	15.157	...
118	08/09/05	53621.2519	53621.2831	130	246	20	1.892	12.300	...
119	11/09/05	53624.0791	53624.0902	107	200	22	1.869	9.090	...
120	12/09/05	53625.1170	53625.1407	105	214	29	2.038	7.379	...
121	13/09/05	53626.2309	53626.2630	97	191	28	1.969	6.821	...
122	14/09/05	53627.4739	53627.6011	93	205	35	2.204	5.857	...
123	15/09/05	53628.1961	53628.2271	84	233	49	2.776	4.758	13.14
124	15/09/05	53628.5898	53628.6015	74	229	52	3.105	4.412	12.72
125	15/09/05	53628.9169	53628.9320	59	222	60	3.715	3.642	9.863, 20.20

^{a}Ratio of 3.5-10.5 keV and 2-3.5 keV PCA count rates.

^{b}Ratio of 3.5-10.5 keV and 10.5-60 keV PCA count rates.

Table 1. Continued.

Obs. (1)	UT Date (2)	MJD Start (3)	MJD Stop (4)	PCA 2-3.5 keV (5)	PCA 3.5-10.5 keV (6)	PCA 10.5-60 keV (7)	$HR5^a$ (8)	$HR6^b$ (9)	QPO Frequency (10)
126	15/09/05	53628.9830	53628.9994	62	225	59	3.603	3.771	10.40
127	16/09/05	53629.3759	53629.4105	58	220	60	3.762	3.625	9.749, 19.40
128	17/09/05	53630.4898	53630.5299	48	194	60	4.034	3.243	0.207, 8.701, 17.39
129	18/09/05	53631.4734	53631.5125	39	170	57	4.301	2.939	7.823, 15.20
130	19/09/05	53632.4556	53632.4952	27	142	58	5.260	2.417	4.747
131	20/09/05	53633.5037	53633.5438	17	107	54	6.060	1.965	2.216
132	21/09/05	53634.1085	53634.1188	14	92	51	6.571	1.803	1.447
133	21/09/05	53634.3148	53634.3299	13	87	48	6.342	1.783	1.314
134	22/09/05	53635.4695	53635.5091	9	63	41	6.576	1.526	0.584
135	23/09/05	53636.4517	53636.4918	5	43	35	8.638	1.207	0.417
136	25/09/05	53638.3533	53638.3917	5	37	30	6.578	1.212	0.229
137	26/09/05	53639.1382	53639.1688	5	33	28	6.612	1.174	0.205
138	27/09/05	53640.2517	53640.2910	4	28	26	6.472	1.071	0.142
139	28/09/05	53641.0382	53641.0619	4	26	25	6.500	1.040	0.128
140	29/09/05	53642.2828	53642.4539	4	22	24	5.500	0.917	0.102
141	30/10/05	53643.0700	53643.1741	3	21	23	7.000	0.913	0.034, 0.094
142	01/10/05	53644.3135	53644.3531	3	18	22	6.000	0.818	0.073
143	02/10/05	53645.3704	53645.3998	3	17	21	5.667	0.810	0.060
144	03/10/05	53646.2133	53646.2531	3	16	21	5.333	0.762	0.023, 0.054
145	04/10/05	53647.1330	53647.2359	2	14	21	7.000	0.667	0.048
146	05/10/05	53648.1131	53648.1531	2	13	20	6.500	0.650	0.034
147	06/10/05	53649.0376	53649.0915	2	12	19	6.000	0.632	...
148	08/10/05	53651.0607	53651.1720	2	10	19	5.000	0.526	...
149	10/10/05	53653.8863	53653.9193	2	9	17	4.500	0.529	...
150	16/10/05	53659.9037	53659.9498	1	7	17	7.000	0.412	...

^{a}Ratio of 3.5-10.5 keV and 2-3.5 keV PCA count rates.
^{b}Ratio of 3.5-10.5 keV and 10.5-60 keV PCA count rates.

(a) Hard state in the rising phase:

In Figs. 3(a-e), we plot the hardness and softness diagrams along with the light curves in the days when the source exhibited different spectral states. In Fig. 3a and Fig. 3b, the light curves belong to the hard state in the rising phase of the outburst and are of the 10th and the 11th of March, 2005. On the 11th of March, 2005, the photon count is several times than that of the previous day. Though all the three components increased, there is a drastic change in the hardness and the softness ratio diagrams because C was increasing much slower than A and B. Thus the spectrum become much softer within one day. Strong QPO features were observed in both the days. The detailed PDS and spectral features are discussed later below. Interestingly, as will be shown below, on the 11th March of 2005, the source did not exhibit any QPO feature in low energy X-ray (2-4 keV), but it is present in the observation on the 10th of March. Finally, on the 12th March of 2005, the source enters into soft state and the QPO is totally absent. On both the days $B > A > C$.

(b) Soft state in the rising phase:

In Fig. 3c, we draw a similar figure with the data of the 20th of March, 2005, when the source was in the soft state. The C component is further reduced while A and B continue to go up with A approaching B. No QPO signature is observed in this state. In this case $B > A >> C$.

(c) Intermediate state:

In Fig. 3d, we present the light curve and the hardness/softness diagram in the intermediate state as observed in a typical day (17th May, 2005). The C component is increased very rapidly while the others increasing very slowly. This state shows some evidence of QPOs on certain days. Here also $B > A > C$.

(d) Hard state in the decline phase:

Finally, in Fig. 3e, when the source is in the hard state again, both the slopes of the hardness and the softness diagrams are more flat as compared to those in the intermediate state and have a similar characteristics as that of the hard state. A typical case based on the observation on the 17th of September, 2005 is shown here. In this case, the components B and C became dominant are more than the photon counts in A. Here, $B > C > A$. The tendencies of the ratios C/A and B/A in relation to the count rate are consistent with that shown in Figs 3(a-b). Again, QPO has started appearing in this state and the frequency went down as the days progressed.

2.2.2   **Power Density Spectra**

Figures 4-8 show results of the PDS for the entire episode. To generate Power Density Spectrum (PDS), we have used "powspec" task of XRONOS package with a normalization factor of '-2' to have the 'white' noise subtracted rms fractional variability. The power obtained has the unit of rms^2/Hz. The light curve of X-ray variability from which PDS was obtained were binned at 0.01 sec time resolution so that the Nyquist frequency is 50 Hz. QPOs are generally Lorentzian type (Nowak 2000; van der Klis 2005) and thus each PDS was fitted with a power-law plus Lorentzian profile to derive the central frequencies and widths of each observed QPO. One has to be careful in rebinning the frequency scale (Papadakis & Lawrence 1993) as it may misrepresent the behaviour especially at low frequencies. In our case, we rebinned the PDS with a geometrical factor of -1.02 to have a nearly equispaced log(frequency) bin. For this choice, any QPO below 0.0122Hz would not be detected. For the best fitting of the PDS as well as QPO profiles we used the least square fit technique. After fitting PDS, we have used "fit err" task to calculate +/- error for QPO frequencies and widths. This task calculates the 90% confidence range of any fitted parameter. For the best fit we occasionally use another broad Lorentzian component at the break frequency position. In Table 2, we present a summary of the results where we put the centroid frequency (ν) of the QPO, its width ($\Delta\nu$) (both in Hz), the coherence parameter Q ($= \nu/\Delta\nu$). The RMS amplitudes $\mathcal{R}$ of the fitted QPOs are also included which were calculated from $\mathcal{R} = 100(PW\pi/ <\phi>)^{1/2}$, where, P, W and ϕ are the power, half-width ($\Delta\nu/2$) of the Lorentzian fitted QPO and the mean count rate of the source respectively. If $Q > 2$, it is considered to be a strong QPO, otherwise it is not strong and look more like a bump on the PDS. Since we are interested only in the QPO properties, namely, the frequencies associated with the QPO, bump and the break, only these are included in the Table and not the power-law features which may been used for the best fit. Since fitting the total PDS is not our goal, an F-test is not needed to check whether the extra model components are required or not.

In Fig. 4a, we present the model fitted PDS of the light curve of 10th March, 2005 (ID: 90704-04-01-00). We used the "Constant + Lorentzian + Lorentzian + Lorentzian + Power-Law" models for the fitting. QPOs are at 2.313Hz & 4.599Hz with a 0.363Hz break frequency. The higher frequency QPO is clearly the first harmonic frequency. Index of the Power-Law after the break is -0.383. In Fig. 4b, the PDS of 20th March, 2005 (ID: 91702-01-08-00) is shown. This is fitted with "Power-Law + Power-Law" models. This is akin to a soft state PDS. Index of the first Power-Law is $= -0.6339$ and the second power-Law is -0.5767. In Fig. 4c, we show the model fitted PDS in the intermediate-state on 17th May, 2005 (ID: 91702-01-57-00G). We used "Power-Law + Lorentzian + Lorentzian" models for the fitting. Here the QPO frequency of 18.94 Hz with a QPO bump at frequency 7.65 Hz. Index of the first Power-Law is $= -1.299$. In Fig. 4d, the result of 17th September, 2005 (ID: 91702-01-79-00), when the object was in the hard state of the declining phase is shown. We used "Power-Law + Lorentzian + Lorentzian + Lorentzian + Lorentzian + Power-Law" models for the fitting. Here we found QPOs
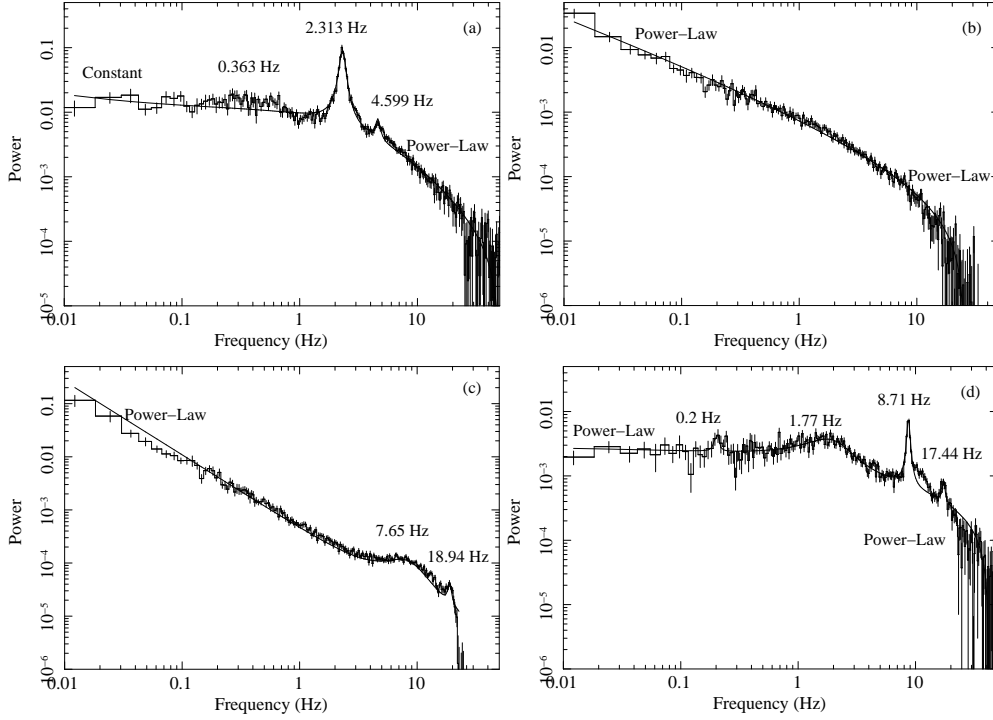
Figure 4. (**a**) The model fitted PDS of 10th March, 2005 (ID: 90704-04-01-00). A QPO is found at 2.313 Hz, with 0.363 Hz break frequency. (**b**) The model fitted PDS of 20th March, 2005 (ID: 91702-01-08-00). No QPO is observed in this case. (**c**) The model fitted PDS of 17th May, 2005 (ID: 91702-01-57-00G). The QPO is at 18.94Hz with a bump at 7.65Hz. (**d**) The model fitted PDS of 17th September, 2005 (ID: 91702-01-79-00). QPOs are found at 0.203Hz, 8.71 Hz with a break frequency at 1.77 Hz.

at frequencies of 0.203Hz, 8.71Hz & 17.39Hz (the last one being a higher harmonic) with a break frequency at 1.77 Hz.

The rising and the declining phases of the outburst showed a very exciting feature. The QPO frequency increased monotonically in the rising phase, while it is decreased monotonically in the declining phase. In Fig. 6 we present the PDS for each day in the rising phase. Arrows indicate the direction in which the date (marked in parenthesis as dd/mm) increases. The observation IDs and the QPO frequencies are also shown in the inset. In Chakrabarti et al. 2005, the trend of the rising phase has been discussed. In Fig. 7, we present the PDS variation in the intermediate state. In the inset we mark frequency at which the bump is formed in case QPO frequency was unavailable. The variation of these frequencies seem to be a bit arbitrary. On the other hand, the variation of PDS in the declining phase (Fig. 8) shows monotonically decreasing QPO frequency. We discuss the implication of these interesting observations in the next Section.
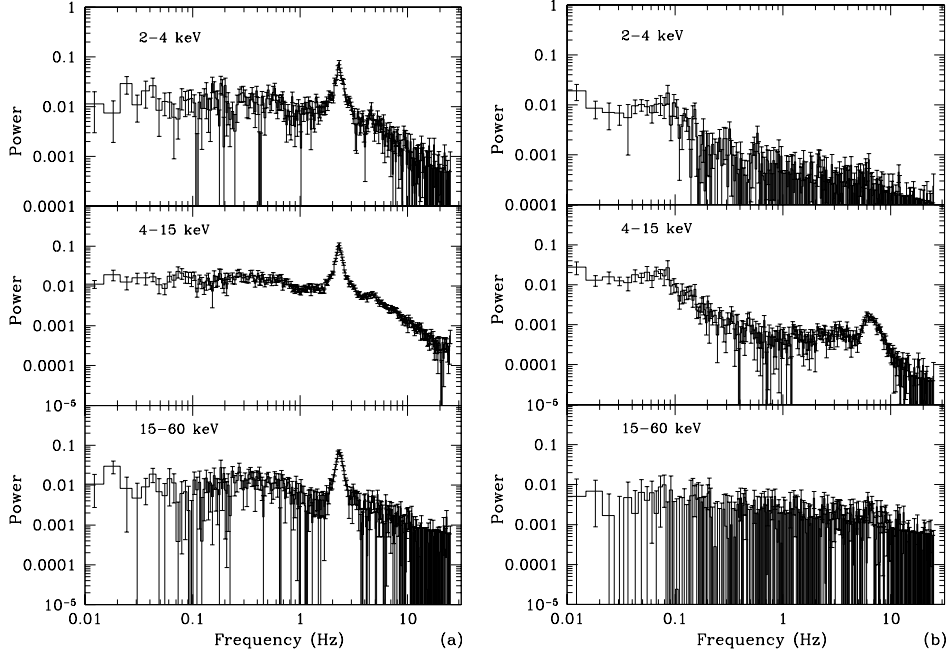
Figure 5. Fig. 5(a-b): Energy dependence of the PDS. The upper, middle and the lower panels are for $2-4$ keV, $4-30$ keV and $30-60$ keV respectively. (a) Data of 10th March, 2005 (ID: 90704-04-01-00). Both the soft and the medium energy X-rays show the 2.313 Hz QPO, the power is higher in medium energy by fifty percent. (b) Data of 11th March, 2005 (ID: 91702-01-02-00G) shows that the QPO at 6.522Hz is exhibited only by hard photons ($4-25$ keV).

2.3 Spectral Analysis

For the spectral analysis we mainly used 3 - 25 keV "**Standard 2**" mode data from RXTE Proportional Counter Unit 2 (PCU2). In general, black hole energy spectra (2-25 keV) are modeled with 'diskbb' and 'power-law' components, though some times best fit could be obtained when a Gaussian around 6.5keV (Iron-line) was used. The results of the 150 PCA observations of 122 days are listed in Table 3. Here, we listed the components required for spectral fits, i.e., the disk black body Temperature T_{in} in keV (Col. 2), normalization factor for black body fit (Col. 3), power-law photon index Γ (Col. 4), power-law normalization (Col. 5), disk black body flux in 3 - 10 keV (Col. 6), the power-law flux in 10 - 25 keV (Col. 7), the total flux in 3 - 25 keV (Col. 8) and the reduced χ^2 (Col. 9). After fitting a spectrum, we have used the "error" command to calculate +/- error for the fitted parameters. All the error values are of 1σ confidence level. For errors bars on flux values, we use flux "LE HE err" to calculate +/- error & flux for the energy range of LE and HE (in keV). We have put the parameter values up to 4 significant digits.
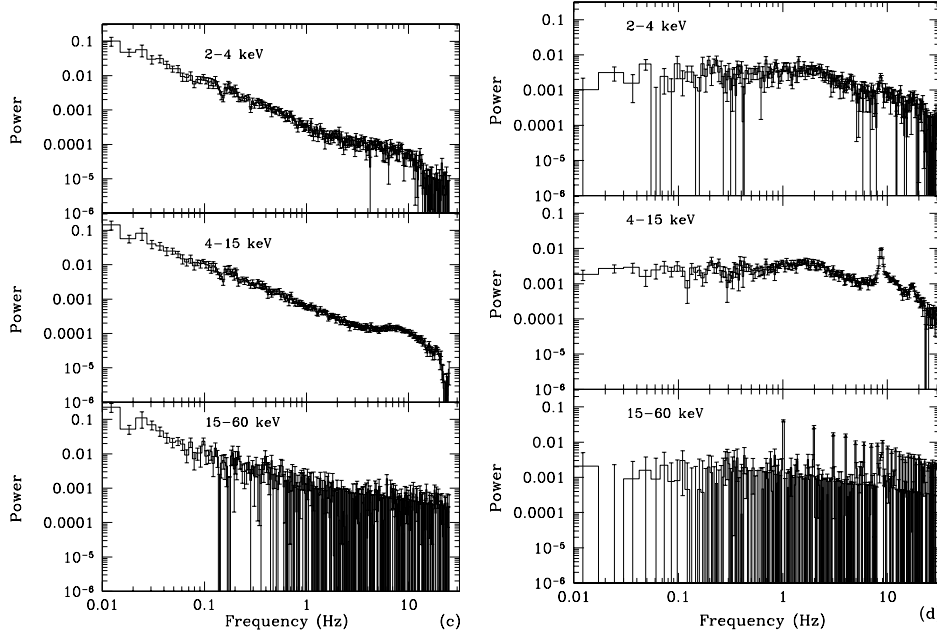
Fig. 5(c-d): (c) PDS of the data of 17th May, 2005 (ID: 91702-01-57-00G) showing that the QPO is exhibited by hard photons (4 - 25 keV) only. (d) PDS of the data of 17th September, 2005 (ID: 91702-01-79-00). Here QPO is seen in both the soft and the intermediate energies as in the hard state of the rising phase (a).

We provide the error bar in each column. The error bars were Fluxes are listed in units of number of photon counts/cm^2/sec. From the nature of the variation of the power-law indices and the disk black body components, we classified the full outburst into four spectral states: (i) Hard state from from 25th of February, 2005 (MJD = 53426) to 12th of March, 2005 (MJD = 53441); (ii) Soft/Very soft state from 13th of March, 2005 (MJD = 53442) to 15th of May, 2005 (MJD = 53505). (iii) Intermediate state is from 16th of May, 2005 (MJD = 53506) to 11th of September, 2005 (MJD = 53624) and finally (iv) Hard state from the 12th of September, 2005 (MJD = 53625) till 16th of October, 2005 (MJD = 53659). We kept the hydrogen column density (N$_H$) fixed at 7.5× 10^{21} atoms cm^{-2} and the systematics at 0.01.

Daily variations of the fitted parameters presented in Table 3 are plotted in Fig. 9 which clearly reveals the justification of separating the full outburst in the above mentioned four states. The panels (a-d) are respectively the black body temperature T_{in} in keV, the black body normalization factor, the photon index Γ and the power-law normalization (plotted in the log scale along Y-axis). Daily variations of the total flux (panel a), black body flux (panel b) and the power-law flux (panel c) are shown in Fig. 10. The panel (d) shows how the ratio of the black body to total flux changes daily. Generally in the soft and very soft states the ratio is almost unity, indicating the dominance of the soft
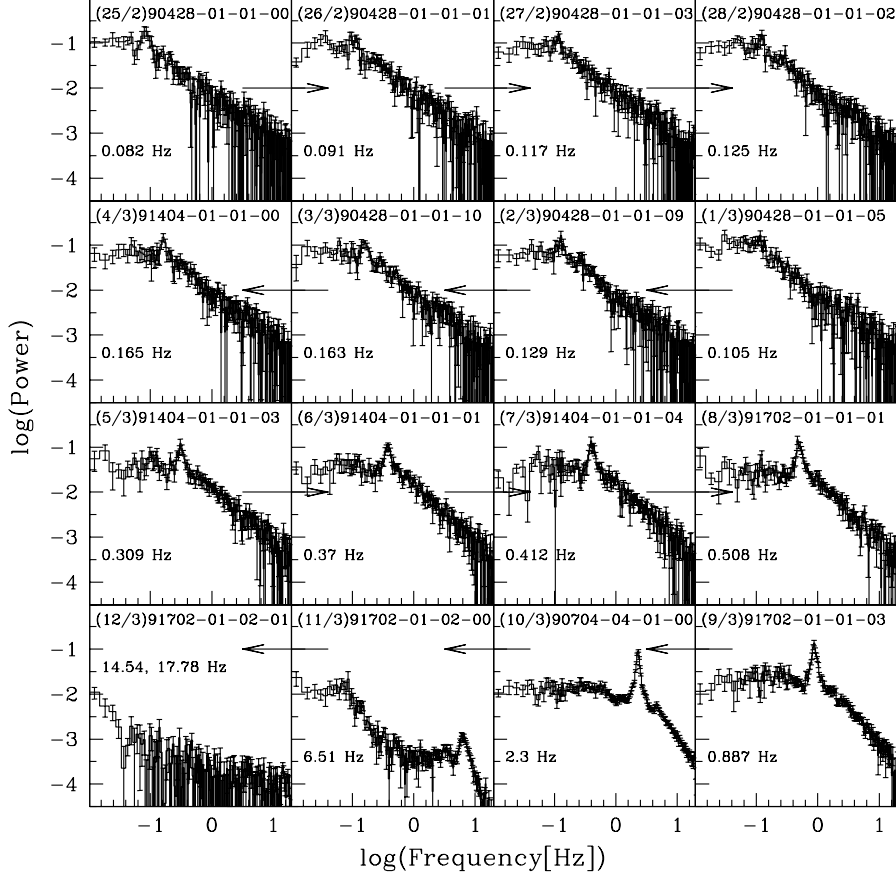
Fig. 6: Variation of the PDS with QPO frequencies marked in the hard state of the rising phase from 25th of February, 2005 to 11th of March, 2005. The dates (dd/mm), the observation ID and the frequency of the QPO are in the inset. Arrows indicate the direction in which the dates are increasing.

component in both of these divisions. However, in Fig. 9, we observe a distinct difference in power-law normalization and power-law index in these two states. The QPOs are observed only in certain days of the intermediate state. It may be noted that Γ obtained right in the middle of the soft/very soft state is unphysically high (> 4). We believe that this is due very poor statistics (e.g., only one good PCU of RXTE was working and photon energy was > 20keV) rather than any unusual absorbtion at high energies. We find that other workers (Saito et al. 2006) also reported a high photon index for these observations.

We have already discussed the daily variation of the spectral index and flux components. It is instructive to study the nature of the complete spectrum itself which we plot in Figs. 11(a-e). In the left panels of each Figure we show the fitted spectrum
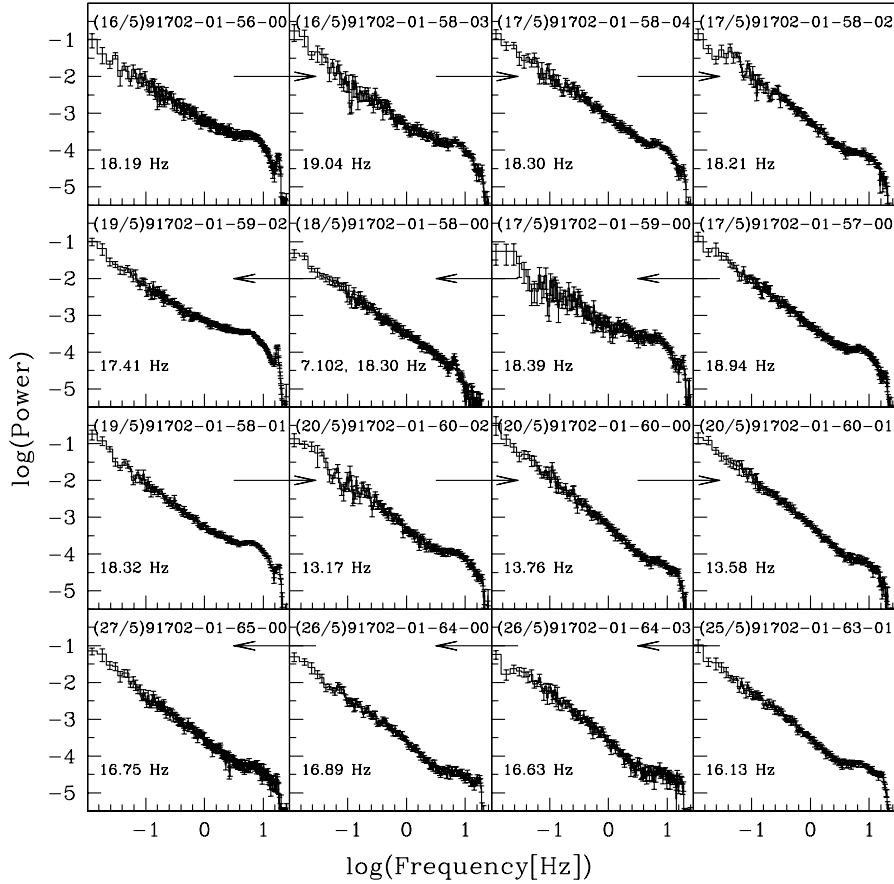
Fig. 7: Same as in Fig. 6, except that the data of the intermediate state from the 16th of May, 2005 to 27th of May, 2005 was chosen.

with individual components (marked on the curves) and in the right panel we show the normalized counts/s/keV and the reduced χ^2_{red} variation. In Fig. 11(e), the component marked 'Compton' comes from fitting with 'CompST' model which represents a Compton cloud which is different from the cloud generating the power-law. These components were chosen so as to get a minimum value of reduced χ^2. To find out the requirement of extra model component to fit the data, is carried out with the F-test task. F-test results are summarized in the Table 4. We chose the combination of the components for which the F-test probability is lowest (see, Col. 6).

Insets show the average χ^2_{red}. The Figures are drawn with data on the 10th March (Id: 90704-04-01-00), (b) 11th March, 2005 (ID: 91702-01-02-00G), (c) 20th March, 2005
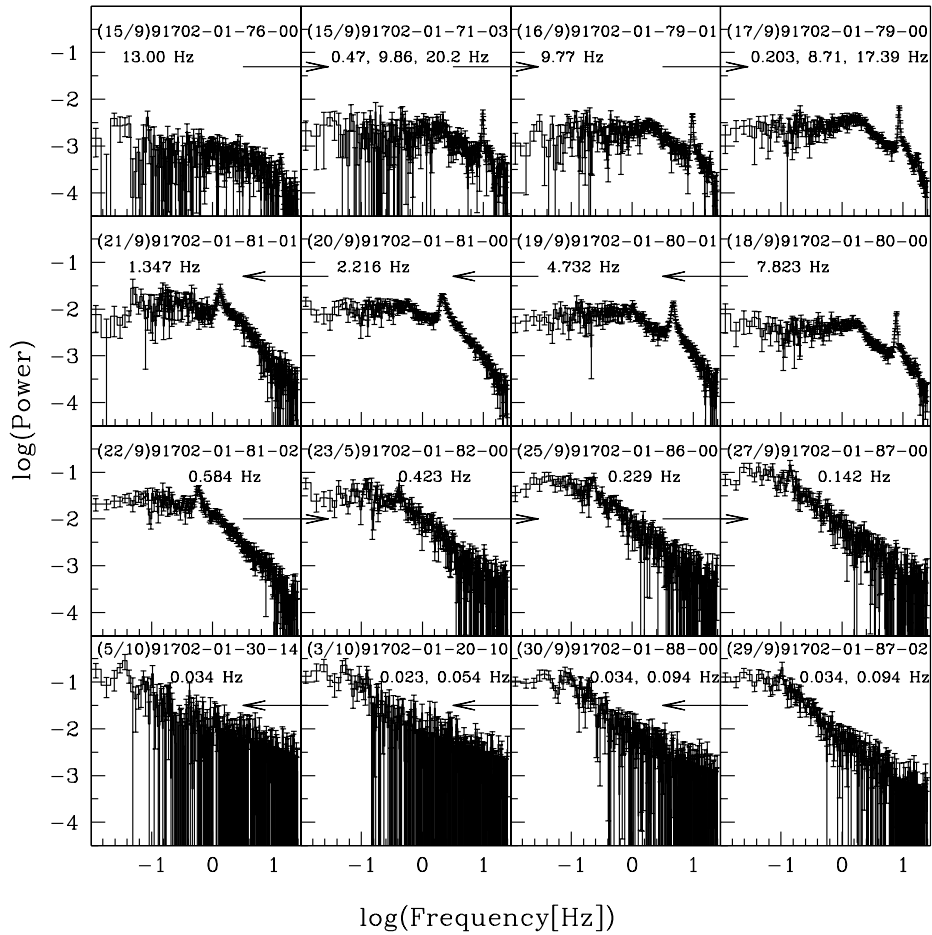
Fig. 8: Same as Fig. 6 except that the data of the decline phase of the outburst from 15th of September, 2005 to 5th of October, 2005 was chosen. Frequency is seen to be decreasing monotonically.

(ID: 91702-01-08-00), (d) 17th May, 2005 (ID: 91702-01-57-00G), and (e) 17th September, 2005 (ID: 91702-01-79-00). Figure symbols have their usual meanings. What we see is that in the hard states the cooler 'Compton' component is missing, while towards the end of the 'intermediate' state and the beginning of the hard state of the decline phase this component shows up, albeit of decreasing importance.
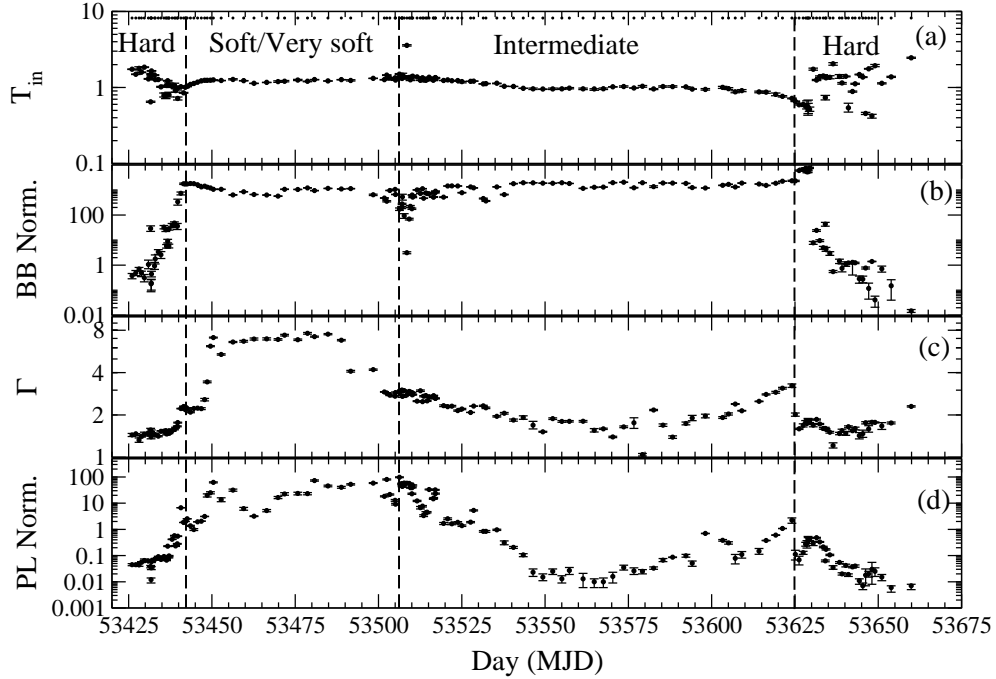
Fig. 9: Fitted parameters of RXTE 3 - 25 keV PCA Spectra plotted with time (MJD). The panels are: (a) disk black body temperature (T_{in}) in keV, (b) disk black body normalization, (c) Power-Law Photon Index (Γ) and (d) Power-Law normalization plotted with day. Logarithmic scale was used in the y-axis and the error bars are at 1σ level.

3.   Brief interpretation of the results

GRO 1655-40 is a typical outburst source which was observed very regularly with one of the most successful X-ray instruments till date. The detailed results of RXTE that we presented reveal several very important aspects of the nature of the transient accretion process around a black hole. From the light curves, hardness/softness diagrams, spectral slopes and most importantly the variation of the QPO frequency, one can come up with very comprehensive picture of what might be happening when such an outburst takes place.

First, we concentrate on the rising and decline phases of the outburst. If we make the most natural assumption that rushing in of matter towards a black hole is the cause of the outburst, then during rising phase the matter is increasing while in the decline phase the matter is evacuated with little fresh supply. The formation of strong QPOs and the smooth variation of QPO frequencies during the outburst (Chakrabarti et al. 2005, 2008) indicates that the cause of QPO is identical each day and is related to the a dynamical property of the infalling matter. While a popular model for low frequency
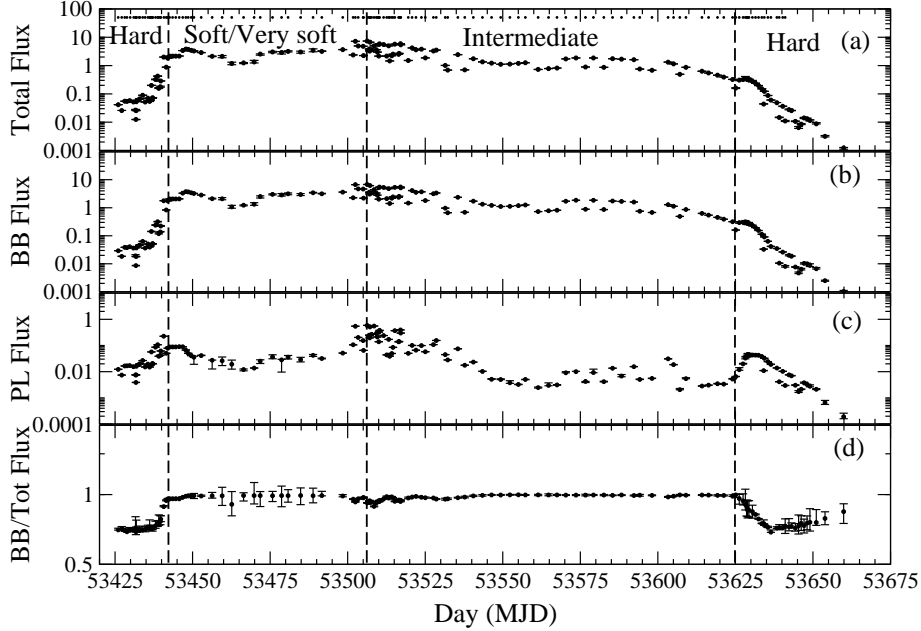
Fig. 10: Derived properties of the daily flux variation are shown. The panels are: (a) 3 - 25 keV total flux, (b) 3-10 keV bolometric disk black body flux, (c) 10-25 keV power-law flux and (d) the ratio of the total and power-law fluxes. In the soft/very soft and intermediate states the total flux is dominated by the black body flux. Only in hard states of the rising and declining phases the ratio is less than unity. Here we use logarithmic scale along the y-axis.

QPO assumes the motion of a perturbation or blob at the inner edge of a Keplerian disk (e.g., Trudolyubov et al. 1999) it is difficult to imagine how a perturbation would sustain itself against shear and dissipation for more than a few orbits, let alone more than two weeks which we observe here. Because of this, we prefer the oscillating shock solution inside a sub-Keplerian disk which has been demonstrated to have a stable oscillation for many dynamical time scale (Molteni, Sponholz & Chakrabarti 1996; Ryu, Chakrabarti & Molteni 1997; Chakrabarti & Manickam, 2000; Chakrabarti, Acharyya & Molteni 2004). It is easy to verify that the QPO frequencies (which are inverses of the infall times from the post-shock flow to the black hole) in the infalling phase are simply related, as though the shock itself is drifting towards the black hole at a slow pace of $\sim 20m/s$ (Chakrabarti et al. 2005). In the decline phase, in the same way, the shock was found to recede, at first very slowly (as though there was still some significant infalling matter) for about three days, and then at an almost constant acceleration (Chakrabarti et al. 2008).

During the onset phase of more than two weeks, the disk got sufficient time to transport angular momentum and a dominant Keplerian disk is formed which made the flow soft or very soft. The rapid rise of the black body flux after the QPO disappears and almost total absence of the hard photons testify to the rushing in of the Keplerian disk

Table 2. Observed QPO fitted parameters.

Obs. (1)	UT Date (2)	ν (3)	$\Delta\nu$ (4)	Q (5)	RMS Amplitude (6)
1	25/02/05	$0.082^{+0.007}_{-0.002}$	$0.018^{+0.013}_{-0.008}$	4.432	6.410
2	26/02/05	$0.034^{+0.011}_{-0.011}$	$0.010^{+0.003}_{-0.002}$	3.269	5.021
2	26/02/05	$0.106^{+0.010}_{-0.025}$	$0.036^{+0.005}_{-0.009}$	2.961	6.852
3	27/02/05	$0.116^{+0.006}_{-0.007}$	$0.017^{+0.005}_{-0.008}$	6.824	4.908
4	27/02/05	$0.051^{+0.012}_{-0.008}$	$0.029^{+0.006}_{-0.007}$	1.735	6.048
4	27/02/05	$0.122^{+0.013}_{-0.004}$	$0.013^{+0.006}_{-0.003}$	9.760	5.312
5	28/02/05	$0.051^{+0.015}_{-0.007}$	$0.015^{+0.004}_{-0.003}$	3.446	3.845
5	28/02/05	$0.121^{+0.009}_{-0.010}$	$0.018^{+0.005}_{-0.005}$	6.612	5.441
6	02/03/05	$0.036^{+0.028}_{-0.003}$	$0.011^{+0.003}_{-0.001}$	3.396	4.464
6	02/03/05	$0.109^{+0.010}_{-0.005}$	$0.028^{+0.037}_{-0.011}$	3.838	5.718
7	02/03/05	$0.045^{+0.005}_{-0.009}$	$0.026^{+0.011}_{-0.010}$	1.744	7.126
7	02/03/05	$0.129^{+0.002}_{-0.003}$	$0.012^{+0.006}_{-0.002}$	10.574	6.191
8	02/03/05	$0.050^{+0.012}_{-0.010}$	$0.050^{+0.017}_{-0.017}$	0.998	8.946
8	02/03/05	$0.117^{+0.003}_{-0.009}$	$0.041^{+0.020}_{-0.007}$	2.875	7.535
9	02/03/05	$0.122^{+0.004}_{-0.004}$	$0.033^{+0.004}_{-0.007}$	3.754	9.433
10	02/03/05	$0.121^{+0.014}_{-0.003}$	$0.061^{+0.014}_{-0.007}$	1.977	7.795
11	03/03/05	$0.163^{+0.008}_{-0.005}$	$0.035^{+0.019}_{-0.016}$	4.644	6.362
12	04/03/05	$0.160^{+0.005}_{-0.004}$	$0.018^{+0.006}_{-0.005}$	8.989	5.673
13	05/03/05	$0.247^{+0.010}_{-0.007}$	$0.088^{+0.050}_{-0.030}$	2.807	8.969
14	05/03/05	$0.116^{+0.000}_{-0.018}$	$0.028^{+0.005}_{-0.006}$	4.099	4.326
14	05/03/05	$0.317^{+0.009}_{-0.007}$	$0.076^{+0.020}_{-0.017}$	4.166	9.335
15	06/03/05	$0.383^{+0.010}_{-0.008}$	$0.102^{+0.035}_{-0.024}$	3.759	10.993
16	07/03/05	$0.417^{+0.012}_{-0.012}$	$0.074^{+0.070}_{-0.031}$	6.608	9.374
17	07/03/05	$0.149^{+0.011}_{-0.005}$	$0.015^{+0.007}_{-0.005}$	10.000	3.684
17	07/03/05	$0.487^{+0.012}_{-0.012}$	$0.074^{+0.070}_{-0.031}$	6.608	9.374
18	07/03/05	$0.125^{+0.003}_{-0.004}$	$0.011^{+0.004}_{-0.003}$	11.792	3.638
18	07/03/05	$0.487^{+0.007}_{-0.005}$	$0.102^{+0.012}_{-0.021}$	4.761	12.329
19	08/03/05	$0.119^{+0.002}_{-0.005}$	$0.005^{+0.001}_{-0.001}$	23.800	2.023
19	08/03/05	$0.513^{+0.013}_{-0.007}$	$0.107^{+0.051}_{-0.007}$	4.803	12.926
20	08/03/05	$0.033^{+0.021}_{-0.004}$	$0.007^{+0.001}_{-0.001}$	4.783	4.039
20	08/03/05	$0.517^{+0.007}_{-0.008}$	$0.100^{+0.010}_{-0.030}$	5.149	13.768
21	09/03/05	$0.886^{+0.011}_{-0.006}$	$0.132^{+0.036}_{-0.007}$	6.722	15.537
22	09/03/05	$1.349^{+0.005}_{-0.007}$	$0.213^{+0.013}_{-0.021}$	6.342	19.040
23	10/03/05	$0.089^{+0.006}_{-0.009}$	$0.014^{+0.012}_{-0.007}$	6.449	2.529
23	10/03/05	$1.528^{+0.012}_{-0.009}$	$0.188^{+0.021}_{-0.019}$	8.132	18.639
24	10/03/05	$2.035^{+0.010}_{-0.010}$	$0.243^{+0.025}_{-0.022}$	8.357	19.935
25	10/03/05	$2.313^{+0.008}_{-0.007}$	$0.298^{+0.021}_{-0.023}$	7.762	19.994
25	10/03/05	$4.620^{+0.008}_{-0.006}$	$0.450^{+0.025}_{-0.018}$	10.267	5.317
26	11/03/05	$3.262^{+0.220}_{-0.121}$	$0.989^{+0.083}_{-0.082}$	3.299	2.493
26	11/03/05	$6.546^{+0.072}_{-0.074}$	$2.305^{+0.234}_{-0.234}$	2.840	6.017

Table 2. Continued.

Obs. (1)	UT Date (2)	ν (3)	$\Delta\nu$ (4)	Q (5)	RMS Amplitude (6)
27	12/03/05	$14.54^{+0.320}_{-0.310}$	$1.466^{+0.399}_{-0.354}$	9.915	2.146
27	12/03/05	$17.78^{+0.260}_{-0.360}$	$1.470^{+0.473}_{-0.347}$	12.095	2.149
57	16/05/05	$18.19^{+0.260}_{-0.280}$	$0.922^{+0.236}_{-0.303}$	19.735	0.825
58	16/05/05	$19.04^{+0.180}_{-0.200}$	$1.248^{+0.144}_{-0.216}$	15.256	0.642
59	17/05/05	$18.30^{+0.180}_{-0.250}$	$0.573^{+0.110}_{-0.100}$	31.954	0.502
60	17/05/05	$18.21^{+0.190}_{-0.280}$	$0.701^{+0.022}_{-0.019}$	25.973	0.420
61	17/05/05	$18.94^{+0.120}_{-0.120}$	$0.245^{+0.002}_{-0.002}$	77.212	0.317
62	17/05/05	$18.65^{+0.240}_{-0.170}$	$0.562^{+0.039}_{-0.080}$	33.179	0.722
63	18/05/05	$6.566^{+0.110}_{-0.194}$	$0.721^{+0.076}_{-0.139}$	9.111	0.767
63	18/05/05	$18.30^{+0.190}_{-0.180}$	$3.280^{+0.194}_{-0.267}$	5.579	0.753
64	19/05/05	$17.41^{+0.040}_{-0.040}$	$0.982^{+0.077}_{-0.078}$	17.724	1.459
65	19/05/05	$18.19^{+0.150}_{-0.120}$	$0.817^{+0.321}_{-0.243}$	22.253	0.641
66	20/05/05	$13.17^{+0.450}_{-0.390}$	$3.576^{+0.484}_{-0.314}$	3.683	1.033
67	20/05/05	$13.76^{+0.270}_{-0.340}$	$3.066^{+0.367}_{-0.310}$	4.488	1.097
68	20/05/05	$13.58^{+0.390}_{-0.250}$	$4.007^{+0.306}_{-0.237}$	3.389	1.419
75	25/05/05	$16.13^{+0.320}_{-0.300}$	$4.010^{+0.381}_{-0.196}$	4.022	1.442
76	26/05/05	$16.63^{+0.350}_{-0.510}$	$1.711^{+0.032}_{-0.027}$	9.719	0.696
77	26/05/05	$16.89^{+0.260}_{-0.660}$	$2.343^{+0.238}_{-0.301}$	7.209	1.102
78	27/05/05	$16.75^{+0.290}_{-0.420}$	$2.804^{+0.238}_{-0.380}$	5.974	1.049
123	15/09/05	$13.14^{+0.390}_{-0.250}$	$4.007^{+0.306}_{-0.237}$	3.389	1.419
124	15/09/05	$12.72^{+0.150}_{-0.180}$	$1.212^{+0.752}_{-0.472}$	10.495	4.297
125	15/09/05	$9.863^{+0.039}_{-0.036}$	$0.795^{+0.165}_{-0.131}$	12.406	7.878
125	15/09/05	$20.20^{+0.560}_{-0.420}$	$1.453^{+0.421}_{-0.323}$	13.902	4.192
126	15/09/05	$10.40^{+0.050}_{-0.030}$	$0.783^{+0.164}_{-0.106}$	13.282	6.926
127	16/09/05	$9.749^{+0.030}_{-0.028}$	$0.590^{+0.077}_{-0.071}$	16.529	6.493
127	16/09/05	$19.40^{+0.340}_{-0.370}$	$0.749^{+0.293}_{-0.267}$	25.905	1.680
128	17/09/05	$0.207^{+0.004}_{-0.003}$	$0.011^{+0.001}_{-0.002}$	19.167	0.783
128	17/09/05	$8.701^{+0.016}_{-0.015}$	$0.457^{+0.040}_{-0.037}$	19.060	7.049
128	17/09/05	$17.39^{+0.290}_{-0.330}$	$0.900^{+0.023}_{-0.017}$	19.322	2.711
129	18/09/05	$7.823^{+0.018}_{-0.018}$	$0.500^{+0.052}_{-0.048}$	15.663	7.737
129	18/09/05	$15.20^{+0.280}_{-0.330}$	$0.898^{+0.145}_{-0.031}$	16.927	2.760
130	19/09/05	$4.747^{+0.023}_{-0.022}$	$0.677^{+0.074}_{-0.066}$	7.007	10.922
131	20/09/05	$2.216^{+0.249}_{-0.203}$	$0.821^{+0.038}_{-0.027}$	2.700	15.105
132	21/09/05	$1.447^{+0.029}_{-0.025}$	$0.579^{+0.141}_{-0.103}$	2.501	13.857
133	21/09/05	$1.314^{+0.011}_{-0.010}$	$0.316^{+0.029}_{-0.018}$	4.160	10.945
134	22/09/05	$0.584^{+0.014}_{-0.022}$	$0.140^{+0.023}_{-0.028}$	4.163	9.732
135	23/09/05	$0.417^{+0.018}_{-0.023}$	$0.296^{+0.119}_{-0.065}$	1.409	12.048
136	25/09/05	$0.229^{+0.015}_{-0.012}$	$0.114^{+0.086}_{-0.053}$	2.005	10.331
137	26/09/05	$0.205^{+0.007}_{-0.006}$	$0.144^{+0.028}_{-0.022}$	1.427	11.792
138	27/09/05	$0.142^{+0.016}_{-0.004}$	$0.004^{+0.001}_{-0.001}$	39.444	2.583

Table 2. Continued.

Obs. (1)	UT Date (2)	ν (3)	$\Delta\nu$ (4)	Q (5)	RMS Amplitude (6)
139	28/09/05	$0.128^{+0.010}_{-0.008}$	$0.042^{+0.007}_{-0.003}$	3.070	7.682
140	29/09/05	$0.102^{+0.011}_{-0.003}$	$0.024^{+0.011}_{-0.005}$	4.232	8.701
141	30/10/05	$0.034^{+0.004}_{-0.003}$	$0.021^{+0.001}_{-0.002}$	1.650	6.592
141	30/10/05	$0.094^{+0.004}_{-0.005}$	$0.065^{+0.006}_{-0.005}$	1.440	11.400
142	01/10/05	$0.073^{+0.006}_{-0.004}$	$0.062^{+0.006}_{-0.002}$	1.185	11.902
143	02/10/05	$0.060^{+0.006}_{-0.005}$	$0.045^{+0.005}_{-0.004}$	1.342	11.677
144	03/10/05	$0.023^{+0.005}_{-0.003}$	$0.013^{+0.004}_{-0.003}$	1.729	6.633
144	03/10/05	$0.054^{+0.005}_{-0.005}$	$0.023^{+0.006}_{-0.003}$	2.379	8.649
145	04/10/05	$0.048^{+0.003}_{-0.008}$	$0.042^{+0.005}_{-0.003}$	1.151	10.512
146	05/10/05	$0.034^{+0.005}_{-0.004}$	$0.019^{+0.002}_{-0.006}$	1.744	8.707

towards the inner edge (Chakrabarti & Titarchuk 1995; Ebisawa et al. 1996). If we take the two component advective flow (TCAF) model one step further and actually fit the spectra of a few days spreaded during the outburst we observe, using the same procedure that was followed in Chakrabarti & Mandal (2006), we can obtain the accretions rates of matter in the Keplerian disk and the sub-Keplerian halo. Table 5 gives the rates in units of Eddington rate on various days. It is clear that the Keplerian disk rate steady increases from the beginning while the halo rate changes in a shorter time scale. At the beginning, the halo rate was higher than the disk rate, but in the rest of the time, until the very end the disk rate always dominates. In the soft and the very soft states, the disk rate required to fit the spectra can be high reaching to about two Eddington rates. The hardness/softness diagrams also give an idea of how the accretion rates in the Keplerian and sub-Keplerian components could be changed on a daily basis. After the very soft state is passed, the viscous processes became weaker and inflowing matter which continues to accrete sporadically becomes dominant. The count rate rapidly fell from tens of thousands to a few hundreds. QPOs started appearing only sporadically in this state. The general trend of the declining inflow rate together with the lowering of viscosity ensured the sucking in of the Keplerian matter. In the hard state of the declining phase, the sub-Keplerian component became comparable to the Keplerian rate giving rise to a strong power-law flux and QPOs.

In the literature, there are reports of other sources which exhibited similar outbursts. For XTE J1550-564, a similar interpretation with TCAF and shock waves was found to be very successful (Soria et al. 2001; Wu et al. 2002, Chakrabarti, Datta & Pal 2009). The spectral state transitions in outburst sources appear to be fundamentally different from those in a persistent source (such as Cyg X-1). In the latter case, the total flux could be almost constant even during the state transitions (Zhang et al. 1996) where the Keplerian and the sub-Keplerian rates could be redistributed during the state transition

Table 3. PCA Spectral fitted parameters.

Obs. (1)	diskbb $T_{in}(keV)$ (2)	diskbb Norm. (3)	Power-Law Index(Γ) (4)	Power-Law Norm. (5)	Black Body Flux[d] (6)	Power-Law Flux[e] (7)	Total Flux[f] (8)	$\chi^2_{red.}$ (9)
1[a]	$1.738^{+0.012}_{-0.012}$	$0.379^{+0.092}_{-0.085}$	$1.442^{+0.036}_{-0.035}$	$0.045^{+0.004}_{-0.004}$	$0.0292^{+0.0007}_{-0.0007}$	$0.0123^{+0.0001}_{-0.0001}$	$0.0415^{+0.0004}_{-0.0004}$	1.133
2[a]	$1.494^{+0.011}_{-0.011}$	$0.495^{+0.112}_{-0.114}$	$1.469^{+0.003}_{-0.003}$	$0.045^{+0.004}_{-0.004}$	$0.0184^{+0.0006}_{-0.0006}$	$0.0074^{+0.0002}_{-0.0002}$	$0.0258^{+0.0002}_{-0.0004}$	1.051
3[a]	$1.785^{+0.088}_{-0.089}$	$0.703^{+0.105}_{-0.104}$	$1.326^{+0.048}_{-0.046}$	$0.044^{+0.005}_{-0.005}$	$0.0386^{+0.0002}_{-0.0002}$	$0.0166^{+0.0002}_{-0.0002}$	$0.0551^{+0.0004}_{-0.0003}$	1.026
4[b]	$1.588^{+0.018}_{-0.011}$	$0.482^{+0.134}_{-0.094}$	$1.411^{+0.019}_{-0.018}$	$0.056^{+0.002}_{-0.003}$	$0.0375^{+0.0013}_{-0.0013}$	$0.0168^{+0.0001}_{-0.0001}$	$0.0543^{+0.0001}_{-0.0010}$	0.601
5[b]	$1.848^{+0.018}_{-0.019}$	$0.314^{+0.109}_{-0.098}$	$1.460^{+0.044}_{-0.049}$	$0.065^{+0.007}_{-0.007}$	$0.0406^{+0.0004}_{-0.0004}$	$0.0171^{+0.0004}_{-0.0004}$	$0.0577^{+0.0002}_{-0.0012}$	1.071
6[b]	$1.294^{+0.012}_{-0.016}$	$1.063^{+0.521}_{-0.342}$	$1.470^{+0.021}_{-0.023}$	$0.062^{+0.004}_{-0.004}$	$0.0365^{+0.0004}_{-0.0004}$	$0.0155^{+0.0002}_{-0.0002}$	$0.0519^{+0.0005}_{-0.0005}$	1.055
7[b]	$0.647^{+0.010}_{-0.013}$	$29.060^{+6.762}_{-7.942}$	$1.565^{+0.042}_{-0.041}$	$0.038^{+0.004}_{-0.004}$	$0.0192^{+0.0008}_{-0.0008}$	$0.0075^{+0.0005}_{-0.0005}$	$0.0267^{+0.0017}_{-0.0014}$	0.624
8[b]	$1.499^{+0.013}_{-0.018}$	$0.180^{+0.093}_{-0.082}$	$1.398^{+0.045}_{-0.047}$	$0.012^{+0.003}_{-0.003}$	$0.0086^{+0.0002}_{-0.0002}$	$0.0039^{+0.0001}_{-0.0001}$	$0.0125^{+0.0002}_{-0.0002}$	0.967
9[b]	$1.408^{+0.026}_{-0.040}$	$0.192^{+0.091}_{-0.080}$	$1.524^{+0.041}_{-0.047}$	$0.034^{+0.005}_{-0.004}$	$0.0181^{+0.0001}_{-0.0001}$	$0.0075^{+0.0001}_{-0.0001}$	$0.0256^{+0.0004}_{-0.0004}$	0.856
10[b]	$1.651^{+0.011}_{-0.018}$	$0.442^{+0.102}_{-0.080}$	$1.445^{+0.028}_{-0.029}$	$0.059^{+0.005}_{-0.005}$	$0.0369^{+0.0023}_{-0.0033}$	$0.0161^{+0.0002}_{-0.0001}$	$0.0529^{+0.0022}_{-0.0036}$	0.664
11[b]	$1.458^{+0.021}_{-0.014}$	$0.922^{+0.245}_{-0.365}$	$1.447^{+0.024}_{-0.022}$	$0.071^{+0.004}_{-0.004}$	$0.0449^{+0.0006}_{-0.0009}$	$0.0192^{+0.0002}_{-0.0002}$	$0.0641^{+0.0006}_{-0.0008}$	0.577
12[b]	$1.267^{+0.012}_{-0.014}$	$1.775^{+0.655}_{-0.779}$	$1.448^{+0.022}_{-0.019}$	$0.074^{+0.005}_{-0.004}$	$0.0467^{+0.0013}_{-0.0016}$	$0.0199^{+0.0001}_{-0.0001}$	$0.0666^{+0.0009}_{-0.0017}$	0.669
13[b]	$1.273^{+0.017}_{-0.022}$	$3.404^{+0.721}_{-0.765}$	$1.414^{+0.014}_{-0.011}$	$0.091^{+0.003}_{-0.003}$	$0.0628^{+0.0004}_{-0.0014}$	$0.0267^{+0.0002}_{-0.0001}$	$0.0895^{+0.0005}_{-0.0004}$	0.598
14[b]	$1.018^{+0.013}_{-0.016}$	$2.602^{+0.753}_{-0.867}$	$1.530^{+0.015}_{-0.017}$	$0.071^{+0.003}_{-0.003}$	$0.0364^{+0.0005}_{-0.0005}$	$0.0151^{+0.0001}_{-0.0002}$	$0.0515^{+0.0009}_{-0.0008}$	0.671
15[b]	$0.784^{+0.062}_{-0.034}$	$32.880^{+4.692}_{-5.130}$	$1.535^{+0.021}_{-0.017}$	$0.092^{+0.004}_{-0.004}$	$0.0509^{+0.0009}_{-0.0008}$	$0.0194^{+0.0002}_{-0.0001}$	$0.0703^{+0.0006}_{-0.0008}$	1.226
16[b]	$0.779^{+0.065}_{-0.066}$	$25.730^{+3.612}_{-2.320}$	$1.547^{+0.020}_{-0.019}$	$0.074^{+0.004}_{-0.003}$	$0.0392^{+0.0033}_{-0.0035}$	$0.0149^{+0.0001}_{-0.0001}$	$0.0542^{+0.0004}_{-0.0010}$	0.879
17[b]	$1.061^{+0.010}_{-0.012}$	$5.814^{+1.032}_{-0.835}$	$1.466^{+0.022}_{-0.024}$	$0.067^{+0.003}_{-0.006}$	$0.0426^{+0.0013}_{-0.0020}$	$0.0172^{+0.0002}_{-0.0003}$	$0.0598^{+0.0008}_{-0.0008}$	0.945
18[b]	$1.228^{+0.016}_{-0.012}$	$9.005^{+1.282}_{-1.717}$	$1.476^{+0.015}_{-0.013}$	$0.228^{+0.006}_{-0.009}$	$0.1421^{+0.0026}_{-0.0013}$	$0.0567^{+0.0003}_{-0.0007}$	$0.1988^{+0.0028}_{-0.0029}$	0.571
19[b]	$1.082^{+0.056}_{-0.012}$	$5.845^{+0.976}_{-1.006}$	$1.485^{+0.013}_{-0.017}$	$0.085^{+0.004}_{-0.003}$	$0.0513^{+0.0005}_{-0.0005}$	$0.0204^{+0.0007}_{-0.0005}$	$0.0717^{+0.0007}_{-0.0010}$	0.632
20[b]	$0.802^{+0.064}_{-0.051}$	$28.660^{+3.654}_{-2.950}$	$1.545^{+0.012}_{-0.015}$	$0.097^{+0.003}_{-0.004}$	$0.0523^{+0.0005}_{-0.0006}$	$0.0199^{+0.0003}_{-0.0003}$	$0.0722^{+0.0009}_{-0.0011}$	0.727
21[b]	$1.038^{+0.038}_{-0.041}$	$38.700^{+7.254}_{-7.413}$	$1.543^{+0.010}_{-0.012}$	$0.418^{+0.010}_{-0.010}$	$0.2373^{+0.0094}_{-0.0094}$	$0.0862^{+0.0003}_{-0.0003}$	$0.3235^{+0.0071}_{-0.0089}$	0.543
22[b]	$1.067^{+0.057}_{-0.070}$	$47.860^{+5.027}_{-5.570}$	$1.579^{+0.013}_{-0.011}$	$0.572^{+0.016}_{-0.017}$	$0.3160^{+0.0052}_{-0.0084}$	$0.1071^{+0.0003}_{-0.0003}$	$0.4231^{+0.0087}_{-0.0104}$	0.535

Fitted with [a] diskbb + power law, [b] diskbb + Gaussian + powerlaw and [c] diskbb + compST + power law
[d] PCA 3-10 keV, [e] PCA 10-25 keV & [f] PCA 3-25 keV Model Fitted Photon Fluxes in number of photons/cm^2/s.

Table 3. Continued.

Obs. (1)	diskbb $T_{in}(keV)$ (2)	diskbb Norm. (3)	Power-Law Index(Γ) (4)	Power-Law Norm. (5)	Black Body Flux^d (6)	Power-Law Flux^e (7)	Total Flux^f (8)	$\chi^2_{red.}$ (9)
23^b	$0.909^{+0.041}_{-0.053}$	$41.600^{+5.378}_{-3.410}$	$1.624^{+0.011}_{-0.012}$	$0.234^{+0.010}_{-0.008}$	$0.1182^{+0.0072}_{-0.0086}$	$0.0387^{+0.0005}_{-0.0008}$	$0.1569^{+0.0023}_{-0.0086}$	0.812
24^b	$0.973^{+0.048}_{-0.054}$	$35.670^{+9.348}_{-10.50}$	$1.662^{+0.011}_{-0.014}$	$0.282^{+0.011}_{-0.011}$	$0.1365^{+0.0076}_{-0.0067}$	$0.0419^{+0.0008}_{-0.0014}$	$0.1785^{+0.0075}_{-0.0096}$	0.812
25^b	$0.717^{+0.033}_{-0.032}$	$335.00^{+87.65}_{-92.52}$	$1.766^{+0.010}_{-0.013}$	$0.549^{+0.013}_{-0.015}$	$0.2229^{+0.0067}_{-0.0088}$	$0.0617^{+0.0003}_{-0.0024}$	$0.2846^{+0.0024}_{-0.0039}$	1.020
26^b	$1.024^{+0.030}_{-0.025}$	$735.70^{+100.5}_{-93.14}$	$2.220^{+0.011}_{-0.018}$	$6.702^{+0.018}_{-0.020}$	$1.7669^{+0.0021}_{-0.0219}$	$0.2254^{+0.0005}_{-0.0007}$	$1.9923^{+0.0027}_{-0.0143}$	0.875
27^b	$0.851^{+0.012}_{-0.012}$	$1772.3^{+108.6}_{-116.4}$	$2.297^{+0.018}_{-0.020}$	$1.833^{+0.012}_{-0.012}$	$0.8288^{+0.0029}_{-0.0057}$	$0.0503^{+0.0004}_{-0.0003}$	$0.8791^{+0.0021}_{-0.0059}$	1.386
28^b	$1.006^{+0.009}_{-0.009}$	$1727.6^{+90.25}_{-88.34}$	$2.182^{+0.025}_{-0.023}$	$2.007^{+0.014}_{-0.014}$	$1.7533^{+0.0083}_{-0.0067}$	$0.0782^{+0.0005}_{-0.0003}$	$1.8315^{+0.0115}_{-0.0075}$	0.938
29^b	$1.035^{+0.013}_{-0.013}$	$1739.4^{+89.99}_{-87.66}$	$2.228^{+0.019}_{-0.014}$	$2.541^{+0.014}_{-0.013}$	$2.0605^{+0.0055}_{-0.0125}$	$0.0879^{+0.0002}_{-0.0003}$	$2.1485^{+0.0095}_{-0.0075}$	0.564
30^b	$1.097^{+0.018}_{-0.010}$	$1807.7^{+62.76}_{-66.35}$	$2.093^{+0.018}_{-0.016}$	$1.366^{+0.058}_{-0.064}$	$2.0605^{+0.0265}_{-0.0395}$	$0.0879^{+0.0003}_{-0.0020}$	$2.1485^{+0.0085}_{-0.0245}$	0.727
31^b	$1.128^{+0.013}_{-0.013}$	$1776.3^{+54.38}_{-42.48}$	$2.225^{+0.025}_{-0.028}$	$0.986^{+0.077}_{-0.081}$	$2.0611^{+0.0079}_{-0.0161}$	$0.0879^{+0.0022}_{-0.0023}$	$2.1491^{+0.0101}_{-0.0069}$	0.554
32^b	$1.177^{+0.005}_{-0.007}$	$1608.8^{+55.67}_{-47.46}$	$2.236^{+0.024}_{-0.025}$	$1.950^{+0.015}_{-0.014}$	$2.0649^{+0.0031}_{-0.0299}$	$0.0899^{+0.0007}_{-0.0014}$	$2.1548^{+0.0012}_{-0.0328}$	0.725
33^b	$1.223^{+0.018}_{-0.018}$	$1320.6^{+46.12}_{-39.85}$	$2.218^{+0.033}_{-0.034}$	$2.054^{+0.022}_{-0.020}$	$3.3043^{+0.0117}_{-0.0123}$	$0.0890^{+0.0005}_{-0.0021}$	$3.3934^{+0.0106}_{-0.0174}$	0.577
34^b	$1.243^{+0.021}_{-0.018}$	$1415.7^{+33.86}_{-21.01}$	$2.569^{+0.054}_{-0.053}$	$3.119^{+0.051}_{-0.048}$	$3.7548^{+0.0122}_{-0.0158}$	$0.0668^{+0.0005}_{-0.0009}$	$3.8163^{+0.0207}_{-0.0103}$	0.598
35^b	$1.241^{+0.012}_{-0.009}$	$1296.4^{+18.34}_{-17.28}$	$3.437^{+0.047}_{-0.048}$	$19.92^{+2.659}_{-2.748}$	$3.6660^{+0.0120}_{-0.0150}$	$0.0501^{+0.0004}_{-0.0006}$	$3.7161^{+0.0089}_{-0.0221}$	1.540
36^b	$1.245^{+0.015}_{-0.012}$	$1200.3^{+20.03}_{-19.20}$	$6.164^{+0.055}_{-0.053}$	$25.01^{+2.368}_{-2.351}$	$3.4127^{+0.0223}_{-0.0457}$	$0.0407^{+0.0006}_{-0.0008}$	$3.4534^{+0.0246}_{-0.0564}$	2.211
37^a	$1.258^{+0.009}_{-0.003}$	$1065.1^{+19.49}_{-21.76}$	$7.093^{+0.047}_{-0.049}$	$62.45^{+2.961}_{-3.008}$	$3.2324^{+0.0756}_{-0.0498}$	$0.0356^{+0.0094}_{-0.0006}$	$3.2679^{+0.1061}_{-0.0921}$	1.941
38^a	$1.236^{+0.008}_{-0.002}$	$1066.0^{+16.68}_{-17.23}$	$5.384^{+0.060}_{-0.059}$	$13.75^{+2.318}_{-2.295}$	$2.8320^{+0.0170}_{-0.0190}$	$0.0413^{+0.0004}_{-0.0013}$	$2.8734^{+0.0076}_{-0.0304}$	2.146
39^a	$1.275^{+0.010}_{-0.029}$	$635.70^{+15.82}_{-12.18}$	$6.603^{+0.056}_{-0.055}$	$31.51^{+2.851}_{-2.976}$	$2.0975^{+0.0415}_{-0.0925}$	$0.0273^{+0.0036}_{-0.0046}$	$2.1248^{+0.0522}_{-0.0508}$	1.815
40^a	$1.231^{+0.010}_{-0.003}$	$843.84^{+12.04}_{-13.20}$	$6.681^{+0.088}_{-0.091}$	$6.206^{+0.810}_{-0.710}$	$2.0831^{+0.1559}_{-0.2071}$	$0.0260^{+0.0020}_{-0.0022}$	$2.1092^{+0.2218}_{-0.1582}$	1.591
41^a	$1.135^{+0.009}_{-0.003}$	$658.60^{+10.67}_{-10.42}$	$6.928^{+0.112}_{-0.116}$	$3.194^{+0.102}_{-0.099}$	$1.0703^{+0.1097}_{-0.1393}$	$0.0192^{+0.0017}_{-0.0014}$	$1.1795^{+0.1105}_{-0.1369}$	1.580
42^a	$1.168^{+0.010}_{-0.003}$	$627.88^{+12.89}_{-12.59}$	$6.944^{+0.123}_{-0.125}$	$5.210^{+0.512}_{-0.498}$	$1.2273^{+0.0397}_{-0.0373}$	$0.0120^{+0.0006}_{-0.0012}$	$1.2394^{+0.0386}_{-0.0324}$	1.105
43^a	$1.194^{+0.025}_{-0.030}$	$568.56^{+12.76}_{-12.55}$	$6.886^{+0.091}_{-0.085}$	$16.41^{+1.492}_{-1.579}$	$1.3286^{+0.1064}_{-0.1840}$	$0.0137^{+0.0007}_{-0.0003}$	$1.3423^{+0.1037}_{-0.1832}$	0.971

Fitted with ^{a} diskbb + power law, ^{b} diskbb + Gaussian + powerlaw and ^{c} diskbb + compST + power law
^{d} PCA 3-10 keV, ^{e} PCA 10-25 keV & ^{f} PCA 3-25 keV Model Fitted Photon Fluxes in number of photons/cm^2/s.

Table 3. Continued.

Obs. (1)	diskbb $T_{in}(keV)$ (2)	diskbb Norm. (3)	Power-Law Index(Γ) (4)	Power-Law Norm. (5)	Black Body Flux[d] (6)	Power-Law Flux[e] (7)	Total Flux[f] (8)	$\chi^2_{red.}$ (9)
44[a]	$1.209^{+0.022}_{-0.027}$	$1065.7^{+21.62}_{-20.78}$	$7.378^{+0.095}_{-0.101}$	$22.52^{+2.439}_{-2.685}$	$2.5168^{+0.1972}_{-0.1426}$	$0.0252^{+0.0016}_{-0.0012}$	$2.5420^{+0.2200}_{-0.0601}$	2.042
45[a]	$1.252^{+0.019}_{-0.027}$	$1049.6^{+23.12}_{-20.24}$	$6.851^{+0.081}_{-0.077}$	$23.59^{+2.799}_{-2.620}$	$2.9965^{+0.1335}_{-0.1158}$	$0.0366^{+0.0013}_{-0.0017}$	$3.0331^{+0.1969}_{-0.1524}$	0.996
46[a]	$1.209^{+0.018}_{-0.028}$	$1208.7^{+22.34}_{-24.06}$	$7.612^{+0.108}_{-0.102}$	$23.18^{+2.318}_{-2.282}$	$2.8576^{+0.2644}_{-0.3369}$	$0.0282^{+0.0015}_{-0.0013}$	$2.8859^{+0.3321}_{-0.2259}$	1.854
47[a]	$1.271^{+0.013}_{-0.009}$	$942.27^{+18.71}_{-19.33}$	$7.205^{+0.062}_{-0.060}$	$73.23^{+4.408}_{-4.222}$	$3.1426^{+0.2354}_{-0.2270}$	$0.0358^{+0.0013}_{-0.0016}$	$3.1784^{+0.1556}_{-0.1607}$	1.811
48[a]	$1.220^{+0.008}_{-0.003}$	$1154.6^{+20.22}_{-20.22}$	$7.506^{+0.077}_{-0.074}$	$45.46^{+3.265}_{-3.244}$	$2.9707^{+0.2503}_{-0.2298}$	$0.0289^{+0.0013}_{-0.0014}$	$2.9996^{+0.2624}_{-0.2374}$	1.081
49[a]	$1.268^{+0.009}_{-0.003}$	$1092.2^{+21.03}_{-21.53}$	$6.800^{+0.066}_{-0.069}$	$40.54^{+3.330}_{-3.299}$	$3.4206^{+0.1156}_{-0.0704}$	$0.0419^{+0.0015}_{-0.0016}$	$3.4625^{+0.3895}_{-0.4235}$	0.845
50[a]	$1.236^{+0.019}_{-0.019}$	$1129.0^{+22.12}_{-22.74}$	$4.089^{+0.057}_{-0.055}$	$52.44^{+3.007}_{-3.122}$	$3.1366^{+0.1226}_{-0.0064}$	$0.0317^{+0.0009}_{-0.0012}$	$3.1684^{+0.1464}_{-0.0086}$	1.297
51[b]	$1.319^{+0.007}_{-0.007}$	$641.910^{+39.780}_{-40.744}$	$4.199^{+0.043}_{-0.045}$	$58.50^{+2.283}_{-2.006}$	$3.6106^{+0.0284}_{-0.0506}$	$0.0512^{+0.0002}_{-0.0006}$	$3.6617^{+0.0293}_{-0.0437}$	2.078
52[a]	$1.267^{+0.005}_{-0.005}$	$476.230^{+10.870}_{-11.470}$	$2.916^{+0.014}_{-0.016}$	$18.29^{+0.832}_{-0.838}$	$2.2675^{+0.0223}_{-0.0105}$	$0.1062^{+0.0006}_{-0.0004}$	$2.3737^{+0.0063}_{-0.0097}$	1.420
53[b]	$1.454^{+0.015}_{-0.021}$	$354.260^{+20.660}_{-20.625}$	$2.867^{+0.014}_{-0.014}$	$80.55^{+3.454}_{-3.452}$	$6.6697^{+0.0287}_{-0.0223}$	$0.5388^{+0.0091}_{-0.0121}$	$7.1781^{+0.0199}_{-0.0241}$	0.949
54[a]	$1.329^{+0.021}_{-0.015}$	$955.720^{+17.230}_{-16.990}$	$2.763^{+0.018}_{-0.017}$	$21.49^{+1.085}_{-1.102}$	$4.7125^{+0.0135}_{-0.0151}$	$0.2024^{+0.0003}_{-0.0006}$	$4.9149^{+0.0171}_{-0.0219}$	0.893
55[a]	$1.338^{+0.017}_{-0.014}$	$1057.30^{+15.430}_{-15.950}$	$2.718^{+0.028}_{-0.026}$	$12.84^{+1.016}_{-0.983}$	$4.6489^{+0.0159}_{-0.0175}$	$0.1537^{+0.0007}_{-0.0003}$	$4.8025^{+0.0155}_{-0.0255}$	1.295
56[a]	$1.252^{+0.012}_{-0.015}$	$661.630^{+11.320}_{-10.920}$	$2.887^{+0.030}_{-0.027}$	$9.196^{+0.705}_{-0.712}$	$2.1902^{+0.0072}_{-0.0068}$	$0.0649^{+0.0004}_{-0.0005}$	$2.2550^{+0.0070}_{-0.0110}$	1.079
57[b]	$1.497^{+0.021}_{-0.026}$	$171.790^{+19.330}_{-18.910}$	$2.877^{+0.015}_{-0.012}$	$97.79^{+3.580}_{-3.322}$	$6.7651^{+0.0271}_{-0.0219}$	$0.5842^{+0.0011}_{-0.0007}$	$7.3493^{+0.0257}_{-0.0293}$	1.043
58[b]	$1.381^{+0.018}_{-0.018}$	$197.650^{+16.980}_{-16.980}$	$2.992^{+0.016}_{-0.015}$	$55.71^{+2.582}_{-2.580}$	$3.5811^{+0.0171}_{-0.0129}$	$0.2482^{+0.0007}_{-0.0009}$	$3.8293^{+0.0097}_{-0.0193}$	1.272
59[b]	$1.351^{+0.019}_{-0.020}$	$199.650^{+16.330}_{-16.347}$	$2.983^{+0.014}_{-0.015}$	$52.79^{+2.102}_{-2.273}$	$3.3968^{+0.0158}_{-0.0082}$	$0.2391^{+0.0006}_{-0.0008}$	$3.6360^{+0.0110}_{-0.0130}$	1.053
60[b]	$1.314^{+0.015}_{-0.017}$	$277.810^{+17.890}_{-16.330}$	$3.002^{+0.016}_{-0.016}$	$44.72^{+2.049}_{-2.102}$	$3.0584^{+0.0124}_{-0.0096}$	$0.1948^{+0.0005}_{-0.0005}$	$3.2532^{+0.0098}_{-0.0162}$	1.213
61[b]	$1.451^{+0.027}_{-0.090}$	$527.820^{+133.40}_{-145.60}$	$2.711^{+0.046}_{-0.049}$	$43.89^{+3.588}_{-2.782}$	$6.1740^{+0.0240}_{-0.0200}$	$0.5125^{+0.0008}_{-0.0009}$	$6.6865^{+0.0255}_{-0.0215}$	0.934
62[b]	$1.378^{+0.034}_{-0.044}$	$94.099^{+20.670}_{-19.530}$	$2.979^{+0.017}_{-0.017}$	$58.96^{+2.833}_{-2.828}$	$3.3644^{+0.0116}_{-0.0224}$	$0.2656^{+0.0005}_{-0.0007}$	$3.6300^{+0.0200}_{-0.0100}$	1.060
63[b]	$3.582^{+0.075}_{-0.063}$	$3.145^{+0.2890}_{-0.2780}$	$2.776^{+0.016}_{-0.018}$	$57.70^{+0.968}_{-0.982}$	$4.4126^{+0.0134}_{-0.0146}$	$0.5514^{+0.0016}_{-0.0020}$	$4.9640^{+0.0160}_{-0.0220}$	1.067
64[b]	$1.357^{+0.076}_{-0.062}$	$69.188^{+5.5600}_{-5.0640}$	$2.937^{+0.018}_{-0.018}$	$57.05^{+1.948}_{-1.994}$	$3.3429^{+0.0091}_{-0.0169}$	$0.2845^{+0.0004}_{-0.0006}$	$3.6274^{+0.0126}_{-0.0174}$	1.054

Fitted with [a] diskbb + power law, [b] diskbb + Gaussian + powerlaw and [c] diskbb + compST + power law
[d] PCA 3-10 keV, [e] PCA 10-25 keV & [f] PCA 3-25 keV Model Fitted Photon Fluxes in number of photons/cm^2/s.

Table 3. Continued.

Obs. (1)	diskbb $T_{in}(keV)$ (2)	diskbb Norm. (3)	Power-Law Index(Γ) (4)	Power-Law Norm. (5)	Black Body Flux[d] (6)	Power-Law Flux[e] (7)	Total Flux[f] (8)	$\chi^2_{red.}$ (9)
65^b	$1.263^{+0.031}_{-0.030}$	$221.317^{+19.330}_{-19.653}$	$2.911^{+0.013}_{-0.013}$	$39.12^{+1.533}_{-1.523}$	$2.7924^{+0.0076}_{-0.0154}$	$0.2118^{+0.0005}_{-0.0004}$	$3.0042^{+0.0078}_{-0.0132}$	1.042
66^b	$1.369^{+0.013}_{-0.013}$	$178.946^{+11.770}_{-11.302}$	$2.882^{+0.017}_{-0.017}$	$22.87^{+1.131}_{-1.139}$	$2.0207^{+0.0083}_{-0.0127}$	$0.1391^{+0.0004}_{-0.0007}$	$2.1598^{+0.0112}_{-0.0108}$	1.346
67^a	$1.391^{+0.010}_{-0.014}$	$629.570^{+15.430}_{-15.540}$	$2.784^{+0.012}_{-0.011}$	$39.28^{+1.300}_{-1.329}$	$5.2499^{+0.0141}_{-0.0159}$	$0.3253^{+0.0005}_{-0.0007}$	$5.5752^{+0.0218}_{-0.0222}$	1.003
68^a	$1.408^{+0.002}_{-0.002}$	$517.747^{+24.050}_{-24.192}$	$2.793^{+0.016}_{-0.017}$	$47.76^{+2.399}_{-2.392}$	$5.4760^{+0.0290}_{-0.0370}$	$0.3773^{+0.0009}_{-0.0013}$	$5.8533^{+0.0197}_{-0.0403}$	0.943
69^a	$1.377^{+0.017}_{-0.017}$	$1008.10^{+15.830}_{-15.440}$	$2.506^{+0.018}_{-0.016}$	$12.18^{+0.633}_{-0.664}$	$5.2928^{+0.0102}_{-0.0238}$	$0.2393^{+0.0005}_{-0.0008}$	$5.5322^{+0.0168}_{-0.0232}$	1.168
70^a	$1.242^{+0.005}_{-0.004}$	$725.758^{+13.950}_{-13.940}$	$2.973^{+0.035}_{-0.036}$	$6.757^{+0.715}_{-0.714}$	$2.1171^{+0.0089}_{-0.0131}$	$0.0436^{+0.0001}_{-0.0001}$	$2.1607^{+0.0083}_{-0.0137}$	1.119
71^a	$1.342^{+0.011}_{-0.011}$	$1122.20^{+15.110}_{-15.950}$	$2.485^{+0.016}_{-0.018}$	$7.717^{+0.532}_{-0.412}$	$4.7955^{+0.0135}_{-0.0155}$	$0.1705^{+0.0003}_{-0.0006}$	$4.9661^{+0.0109}_{-0.0181}$	1.022
72^a	$1.251^{+0.010}_{-0.004}$	$466.970^{+5.800}_{-6.535}$	$2.717^{+0.024}_{-0.027}$	$3.354^{+0.202}_{-0.268}$	$1.4187^{+0.0053}_{-0.0083}$	$0.0387^{+0.0003}_{-0.0003}$	$1.4574^{+0.0046}_{-0.0054}$	1.272
73^a	$1.244^{+0.003}_{-0.013}$	$767.120^{+9.8700}_{-10.200}$	$2.750^{+0.033}_{-0.030}$	$4.363^{+0.372}_{-0.375}$	$2.1767^{+0.0083}_{-0.0077}$	$0.0495^{+0.0002}_{-0.0003}$	$2.2262^{+0.0088}_{-0.0092}$	1.086
74^a	$1.276^{+0.033}_{-0.004}$	$716.590^{+10.890}_{-10.560}$	$2.519^{+0.021}_{-0.019}$	$4.521^{+0.248}_{-0.247}$	$2.4372^{+0.0068}_{-0.0132}$	$0.0846^{+0.0001}_{-0.0003}$	$2.5218^{+0.0082}_{-0.0088}$	1.338
75^a	$1.363^{+0.015}_{-0.007}$	$707.160^{+22.100}_{-18.220}$	$2.667^{+0.013}_{-0.011}$	$33.29^{+1.100}_{-1.116}$	$5.3299^{+0.0211}_{-0.0199}$	$0.3678^{+0.0008}_{-0.0010}$	$5.6977^{+0.0183}_{-0.0207}$	1.157
76^a	$1.245^{+0.016}_{-0.006}$	$525.050^{+12.830}_{-13.160}$	$2.718^{+0.016}_{-0.014}$	$14.64^{+0.582}_{-0.583}$	$2.3528^{+0.0082}_{-0.0078}$	$0.1384^{+0.0002}_{-0.0004}$	$2.4913^{+0.0087}_{-0.0073}$	0.902
77^a	$1.272^{+0.009}_{-0.008}$	$522.180^{+17.690}_{-17.674}$	$2.742^{+0.018}_{-0.017}$	$15.67^{+0.788}_{-0.792}$	$2.5528^{+0.0092}_{-0.0148}$	$0.1419^{+0.0004}_{-0.0006}$	$2.6946^{+0.0114}_{-0.0126}$	1.358
78^a	$1.349^{+0.014}_{-0.007}$	$772.820^{+20.020}_{-20.440}$	$2.629^{+0.014}_{-0.012}$	$32.38^{+1.202}_{-1.144}$	$5.5171^{+0.0219}_{-0.0251}$	$0.3927^{+0.0009}_{-0.0011}$	$5.9098^{+0.0142}_{-0.0238}$	1.461
79^a	$1.341^{+0.018}_{-0.006}$	$893.120^{+19.020}_{-19.250}$	$2.623^{+0.018}_{-0.016}$	$23.26^{+1.104}_{-1.088}$	$5.1239^{+0.0191}_{-0.0229}$	$0.2983^{+0.0007}_{-0.0011}$	$5.4222^{+0.0208}_{-0.0212}$	1.164
80^a	$1.237^{+0.006}_{-0.006}$	$516.400^{+15.360}_{-15.386}$	$2.327^{+0.033}_{-0.032}$	$1.684^{+0.151}_{-0.152}$	$1.4613^{+0.0107}_{-0.0093}$	$0.0500^{+0.0001}_{-0.0004}$	$1.5113^{+0.0097}_{-0.0143}$	1.172
81^a	$1.259^{+0.023}_{-0.003}$	$1437.50^{+19.780}_{-20.260}$	$2.289^{+0.024}_{-0.025}$	$2.548^{+0.187}_{-0.187}$	$4.0999^{+0.0151}_{-0.0189}$	$0.1003^{+0.0002}_{-0.0004}$	$4.2001^{+0.0129}_{-0.0171}$	1.064
82^a	$1.227^{+0.014}_{-0.003}$	$1449.90^{+18.120}_{-19.270}$	$2.309^{+0.026}_{-0.028}$	$1.635^{+0.128}_{-0.130}$	$3.5353^{+0.0107}_{-0.0163}$	$0.0659^{+0.0001}_{-0.0003}$	$3.6013^{+0.0147}_{-0.0073}$	1.016
83^a	$1.233^{+0.017}_{-0.003}$	$1442.10^{+22.550}_{-21.620}$	$2.146^{+0.020}_{-0.022}$	$1.855^{+0.122}_{-0.129}$	$3.6958^{+0.0122}_{-0.0138}$	$0.0993^{+0.0001}_{-0.0004}$	$3.7950^{+0.0073}_{-0.0110}$	1.342
84^a	$1.196^{+0.045}_{-0.004}$	$779.640^{+17.860}_{-17.760}$	$2.205^{+0.023}_{-0.022}$	$1.387^{+0.089}_{-0.086}$	$1.8078^{+0.0082}_{-0.0128}$	$0.0575^{+0.0001}_{-0.0003}$	$1.8653^{+0.0077}_{-0.0123}$	1.281
85^a	$1.205^{+0.003}_{-0.003}$	$1327.61^{+22.220}_{-22.190}$	$2.084^{+0.001}_{-0.001}$	$1.892^{+0.103}_{-0.101}$	$3.1660^{+0.0110}_{-0.0130}$	$0.1079^{+0.0001}_{-0.0003}$	$3.2740^{+0.0110}_{-0.0140}$	1.290

Fitted with [a] diskbb + power law, [b] diskbb + Gaussian + powerlaw and [c] diskbb + compST + power law
[d] PCA 3-10 keV, [e] PCA 10-25 keV & [f] PCA 3-25 keV Model Fitted Photon Fluxes in number of $photons/cm^2/s$.

Table 3. Continued.

Obs. (1)	diskbb $T_{in}(keV)$ (2)	diskbb Norm. (3)	Power-Law Index(Γ) (4)	Power-Law Norm. (5)	Black Body Flux[d] (6)	Power-Law Flux[e] (7)	Total Flux[f] (8)	$\chi^2_{red.}$ (9)
86[a]	$1.212^{+0.004}_{-0.005}$	$1213.20^{+23.490}_{-23.060}$	$2.311^{+0.003}_{-0.002}$	$5.309^{+0.233}_{-0.236}$	$3.3593^{+0.0117}_{-0.0113}$	$0.1552^{+0.0003}_{-0.0004}$	$3.5144^{+0.0126}_{-0.0144}$	1.315
87[a]	$1.115^{+0.009}_{-0.005}$	$455.830^{+17.030}_{-17.780}$	$2.322^{+0.024}_{-0.024}$	$0.838^{+0.061}_{-0.061}$	$0.9664^{+0.0066}_{-0.0099}$	$0.0449^{+0.0001}_{-0.0003}$	$1.0113^{+0.0097}_{-0.0073}$	0.892
88[a]	$1.125^{+0.007}_{-0.007}$	$363.980^{+13.880}_{-13.910}$	$2.248^{+0.028}_{-0.027}$	$0.838^{+0.068}_{-0.064}$	$0.6627^{+0.0049}_{-0.0056}$	$0.0280^{+0.0003}_{-0.0002}$	$0.6907^{+0.0041}_{-0.0043}$	1.000
89[a]	$1.138^{+0.018}_{-0.004}$	$1326.90^{+24.430}_{-23.400}$	$1.955^{+0.021}_{-0.019}$	$0.961^{+0.050}_{-0.050}$	$2.3560^{+0.0090}_{-0.0090}$	$0.0746^{+0.0003}_{-0.0001}$	$2.4306^{+0.0074}_{-0.0116}$	1.245
90[a]	$1.037^{+0.004}_{-0.004}$	$655.430^{+21.080}_{-20.740}$	$2.057^{+0.030}_{-0.027}$	$0.310^{+0.050}_{-0.053}$	$0.6881^{+0.0038}_{-0.0053}$	$0.0176^{+0.0003}_{-0.0001}$	$0.7057^{+0.0054}_{-0.0056}$	1.573
91[a]	$1.032^{+0.003}_{-0.004}$	$1784.55^{+38.032}_{-38.458}$	$1.839^{+0.033}_{-0.032}$	$0.206^{+0.018}_{-0.018}$	$1.7100^{+0.0090}_{-0.0100}$	$0.0232^{+0.0001}_{-0.0001}$	$1.7332^{+0.0088}_{-0.0132}$	0.926
92[a]	$0.975^{+0.003}_{-0.003}$	$1937.33^{+51.890}_{-52.070}$	$1.919^{+0.055}_{-0.052}$	$0.106^{+0.015}_{-0.012}$	$1.3396^{+0.0094}_{-0.0096}$	$0.0102^{+0.0003}_{-0.0002}$	$1.3498^{+0.0112}_{-0.0098}$	1.262
93[a]	$0.961^{+0.021}_{-0.021}$	$1933.70^{+29.220}_{-29.040}$	$1.692^{+0.100}_{-0.110}$	$0.023^{+0.008}_{-0.007}$	$1.2161^{+0.0049}_{-0.0051}$	$0.0051^{+0.0003}_{-0.0003}$	$1.2212^{+0.0038}_{-0.0062}$	1.635
94[a]	$0.954^{+0.011}_{-0.011}$	$1861.10^{+28.040}_{-29.300}$	$1.518^{+0.012}_{-0.012}$	$0.015^{+0.005}_{-0.004}$	$1.1050^{+0.0040}_{-0.0040}$	$0.0050^{+0.0003}_{-0.0003}$	$1.1100^{+0.0030}_{-0.0050}$	1.137
95[a]	$0.958^{+0.017}_{-0.002}$	$1851.60^{+29.480}_{-30.150}$	$1.883^{+0.025}_{-0.024}$	$0.025^{+0.006}_{-0.006}$	$1.1251^{+0.0029}_{-0.0061}$	$0.0038^{+0.0001}_{-0.0007}$	$1.1289^{+0.0031}_{-0.0059}$	0.979
96[a]	$0.960^{+0.017}_{-0.018}$	$1939.30^{+27.820}_{-26.250}$	$1.800^{+0.025}_{-0.023}$	$0.013^{+0.004}_{-0.004}$	$1.1918^{+0.0042}_{-0.0068}$	$0.0033^{+0.0003}_{-0.0003}$	$1.1950^{+0.0059}_{-0.0050}$	1.268
97[a]	$0.979^{+0.021}_{-0.018}$	$1813.30^{+23.840}_{-24.260}$	$1.801^{+0.020}_{-0.022}$	$0.027^{+0.008}_{-0.008}$	$1.2540^{+0.0040}_{-0.0040}$	$0.0050^{+0.0009}_{-0.0009}$	$1.2591^{+0.0049}_{-0.0051}$	1.118
98[a]	$0.959^{+0.021}_{-0.023}$	$1158.20^{+19.530}_{-18.360}$	$1.804^{+0.024}_{-0.023}$	$0.013^{+0.007}_{-0.008}$	$0.7291^{+0.0026}_{-0.0039}$	$0.0025^{+0.0003}_{-0.0001}$	$0.7315^{+0.0083}_{-0.0044}$	1.374
99[b]	$0.957^{+0.039}_{-0.034}$	$1284.70^{+42.070}_{-42.300}$	$1.556^{+0.043}_{-0.016}$	$0.010^{+0.004}_{-0.003}$	$0.7791^{+0.0045}_{-0.0089}$	$0.0029^{+0.0007}_{-0.0008}$	$0.7821^{+0.0076}_{-0.0080}$	1.462
100[a]	$0.963^{+0.021}_{-0.022}$	$1301.30^{+19.880}_{-19.950}$	$1.593^{+0.018}_{-0.016}$	$0.010^{+0.004}_{-0.004}$	$0.8127^{+0.0044}_{-0.0067}$	$0.0031^{+0.0008}_{-0.0008}$	$0.8158^{+0.0026}_{-0.0043}$	1.992
101[a]	$1.022^{+0.003}_{-0.003}$	$1953.60^{+34.780}_{-31.170}$	$1.396^{+0.016}_{-0.007}$	$0.016^{+0.007}_{-0.007}$	$1.7073^{+0.0067}_{-0.0063}$	$0.0091^{+0.0008}_{-0.0009}$	$1.7164^{+0.0046}_{-0.0084}$	1.349
102[a]	$1.029^{+0.021}_{-0.021}$	$2034.60^{+28.240}_{-28.110}$	$1.646^{+0.022}_{-0.024}$	$0.035^{+0.008}_{-0.008}$	$1.8481^{+0.0079}_{-0.0071}$	$0.0099^{+0.0004}_{-0.0003}$	$1.8581^{+0.0059}_{-0.0101}$	1.910
103[a]	$0.984^{+0.004}_{-0.003}$	$1228.10^{+34.020}_{-33.400}$	$1.759^{+0.155}_{-0.150}$	$0.026^{+0.007}_{-0.008}$	$0.8836^{+0.0057}_{-0.0078}$	$0.0042^{+0.0004}_{-0.0004}$	$0.8883^{+0.0067}_{-0.0076}$	1.557
104[a]	$1.037^{+0.022}_{-0.027}$	$1948.50^{+28.350}_{-29.920}$	$1.045^{+0.024}_{-0.020}$	$0.025^{+0.005}_{-0.003}$	$1.8452^{+0.0078}_{-0.0092}$	$0.0092^{+0.0021}_{-0.0010}$	$1.8544^{+0.0066}_{-0.0114}$	1.173
105[a]	$0.957^{+0.018}_{-0.011}$	$1357.70^{+105.50}_{-100.31}$	$2.168^{+0.022}_{-0.033}$	$0.033^{+0.004}_{-0.004}$	$0.8628^{+0.0046}_{-0.0028}$	$0.0042^{+0.0001}_{-0.0011}$	$0.8669^{+0.0096}_{-0.0055}$	1.690
106[a]	$1.029^{+0.021}_{-0.022}$	$1893.30^{+26.440}_{-27.330}$	$1.692^{+0.033}_{-0.035}$	$0.067^{+0.010}_{-0.010}$	$1.7330^{+0.0070}_{-0.0060}$	$0.0135^{+0.0005}_{-0.0004}$	$1.7465^{+0.0055}_{-0.0075}$	1.051

Fitted with [a] diskbb + power law, [b] diskbb + Gaussian + powerlaw and [c] diskbb + compST + power law
[d] PCA 3-10 keV, [e] PCA 10-25 keV & [f] PCA 3-25 keV Model Fitted Photon Fluxes in number of photons/cm^2/s.

Table 3. Continued.

Obs. (1)	diskbb $T_{in}(keV)$ (2)	diskbb Norm. (3)	Power-Law Index(Γ) (4)	Power-Law Norm. (5)	Black Body Flux[d] (6)	Power-Law Flux[e] (7)	Total Flux[f] (8)	$\chi^2_{red.}$ (9)
107[a]	$1.026^{+0.019}_{-0.028}$	$1886.60^{+32.830}_{-32.970}$	$1.392^{+0.029}_{-0.029}$	$0.087^{+0.003}_{-0.003}$	$1.6814^{+0.0146}_{-0.0146}$	$0.0068^{+0.0004}_{-0.0009}$	$1.6882^{+0.0048}_{-0.0092}$	0.849
108[a]	$1.019^{+0.008}_{-0.028}$	$1830.30^{+27.100}_{-27.220}$	$1.740^{+0.039}_{-0.041}$	$0.098^{+0.011}_{-0.011}$	$1.5982^{+0.0068}_{-0.0062}$	$0.0156^{+0.0005}_{-0.0006}$	$1.6137^{+0.0053}_{-0.0067}$	1.102
109[a]	$0.953^{+0.003}_{-0.003}$	$1238.40^{+33.940}_{-34.249}$	$1.902^{+0.080}_{-0.083}$	$0.051^{+0.012}_{-0.013}$	$0.7509^{+0.0061}_{-0.0071}$	$0.0050^{+0.0003}_{-0.0001}$	$0.7559^{+0.0069}_{-0.0050}$	1.342
110[a]	$0.943^{+0.018}_{-0.024}$	$1196.80^{+20.430}_{-19.760}$	$1.965^{+0.057}_{-0.061}$	$0.700^{+0.011}_{-0.011}$	$0.6776^{+0.0026}_{-0.0033}$	$0.0055^{+0.0003}_{-0.0002}$	$0.6831^{+0.0016}_{-0.0030}$	1.338
111[a]	$1.002^{+0.028}_{-0.024}$	$1533.80^{+28.920}_{-30.020}$	$1.918^{+0.028}_{-0.026}$	$0.382^{+0.028}_{-0.032}$	$1.2872^{+0.0048}_{-0.0062}$	$0.0309^{+0.0001}_{-0.0003}$	$1.3181^{+0.0030}_{-0.0049}$	1.005
112[a]	$0.966^{+0.026}_{-0.033}$	$1675.40^{+32.150}_{-32.480}$	$2.032^{+0.034}_{-0.037}$	$0.306^{+0.032}_{-0.030}$	$1.1285^{+0.0055}_{-0.0055}$	$0.0186^{+0.0001}_{-0.0003}$	$1.1471^{+0.0029}_{-0.0061}$	0.967
113[a]	$0.878^{+0.025}_{-0.030}$	$1316.70^{+25.390}_{-32.150}$	$2.392^{+0.014}_{-0.015}$	$0.079^{+0.031}_{-0.031}$	$0.4896^{+0.0012}_{-0.0029}$	$0.0021^{+0.0003}_{-0.0002}$	$0.4917^{+0.0016}_{-0.0051}$	1.596
114[a]	$0.909^{+0.026}_{-0.022}$	$1883.50^{+33.920}_{-24.490}$	$2.142^{+0.010}_{-0.011}$	$0.110^{+0.030}_{-0.030}$	$0.8631^{+0.0028}_{-0.0038}$	$0.0054^{+0.0003}_{-0.0003}$	$0.8685^{+0.0035}_{-0.0050}$	1.510
115[a]	$0.874^{+0.022}_{-0.021}$	$1726.90^{+30.270}_{-30.150}$	$2.500^{+0.014}_{-0.012}$	$0.148^{+0.036}_{-0.039}$	$0.6280^{+0.0028}_{-0.0023}$	$0.0028^{+0.0003}_{-0.0002}$	$0.6308^{+0.0024}_{-0.0032}$	1.611
116[a]	$0.868^{+0.024}_{-0.032}$	$1517.80^{+28.480}_{-28.660}$	$2.800^{+0.023}_{-0.023}$	$0.376^{+0.008}_{-0.008}$	$0.5434^{+0.0023}_{-0.0025}$	$0.0031^{+0.0002}_{-0.0005}$	$0.5464^{+0.0025}_{-0.0026}$	1.291
117[a]	$0.812^{+0.032}_{-0.034}$	$1853.50^{+51.440}_{-52.110}$	$2.900^{+0.045}_{-0.042}$	$0.604^{+0.015}_{-0.016}$	$0.4529^{+0.0025}_{-0.0028}$	$0.0035^{+0.0005}_{-0.0003}$	$0.4564^{+0.0026}_{-0.0026}$	1.855
118[a]	$0.765^{+0.016}_{-0.015}$	$2232.80^{+28.660}_{-27.450}$	$3.100^{+0.044}_{-0.042}$	$1.081^{+0.015}_{-0.014}$	$0.3891^{+0.0018}_{-0.0016}$	$0.0034^{+0.0003}_{-0.0003}$	$0.3925^{+0.0020}_{-0.0020}$	1.685
119[a]	$0.719^{+0.008}_{-0.007}$	$2320.00^{+122.98}_{-123.90}$	$3.226^{+0.088}_{-0.098}$	$2.239^{+0.533}_{-0.514}$	$0.3171^{+0.0006}_{-0.0044}$	$0.0052^{+0.0003}_{-0.0002}$	$0.3224^{+0.0044}_{-0.0043}$	1.153
120[b]	$0.658^{+0.006}_{-0.005}$	$2305.70^{+133.23}_{-133.30}$	$2.014^{+0.055}_{-0.050}$	$0.112^{+0.044}_{-0.047}$	$0.1604^{+0.0015}_{-0.0013}$	$0.0065^{+0.0006}_{-0.0015}$	$0.1609^{+0.0063}_{-0.0047}$	1.334
121[c]	$0.592^{+0.026}_{-0.003}$	$5948.20^{+266.29}_{-274.80}$	$1.594^{+0.016}_{-0.014}$	$0.069^{+0.025}_{-0.018}$	$0.2954^{+0.0170}_{-0.0141}$	$0.0119^{+0.0015}_{-0.0024}$	$0.3073^{+0.0146}_{-0.0107}$	0.902
122[c]	$0.599^{+0.011}_{-0.012}$	$6487.60^{+910.70}_{-912.80}$	$1.685^{+0.042}_{-0.044}$	$0.129^{+0.017}_{-0.017}$	$0.3015^{+0.0084}_{-0.0209}$	$0.0198^{+0.0011}_{-0.0010}$	$0.3213^{+0.0146}_{-0.0218}$	1.149
123[c]	$0.566^{+0.033}_{-0.042}$	$7376.20^{+265.54}_{-265.20}$	$1.766^{+0.055}_{-0.058}$	$0.272^{+0.043}_{-0.047}$	$0.3150^{+0.0297}_{-0.0348}$	$0.0329^{+0.0020}_{-0.0041}$	$0.3479^{+0.0092}_{-0.0155}$	0.848
124[c]	$0.576^{+0.053}_{-0.091}$	$5271.10^{+400.38}_{-408.80}$	$1.739^{+0.012}_{-0.010}$	$0.281^{+0.088}_{-0.091}$	$0.3002^{+0.0391}_{-0.0111}$	$0.0370^{+0.0014}_{-0.0022}$	$0.3372^{+0.0155}_{-0.0254}$	0.771
125[c]	$0.516^{+0.084}_{-0.103}$	$6923.60^{+590.30}_{-595.40}$	$1.823^{+0.066}_{-0.067}$	$0.448^{+0.091}_{-0.088}$	$0.2726^{+0.0244}_{-0.0201}$	$0.0453^{+0.0034}_{-0.0014}$	$0.3178^{+0.0258}_{-0.0314}$	0.919
126[c]	$0.548^{+0.093}_{-0.135}$	$5346.60^{+420.80}_{-419.80}$	$1.786^{+0.077}_{-0.077}$	$0.389^{+0.089}_{-0.092}$	$0.2802^{+0.0264}_{-0.0160}$	$0.0442^{+0.0067}_{-0.0054}$	$0.3244^{+0.0314}_{-0.0301}$	0.876
127[c]	$0.514^{+0.028}_{-0.039}$	$7593.10^{+418.32}_{-417.60}$	$1.803^{+0.036}_{-0.038}$	$0.422^{+0.044}_{-0.047}$	$0.2698^{+0.0126}_{-0.0293}$	$0.0455^{+0.0012}_{-0.0009}$	$0.3152^{+0.0215}_{-0.0192}$	1.187

Fitted with [a] diskbb + power law, [b] diskbb + Gaussian + powerlaw and [c] diskbb + compST + power law

[d] PCA 3-10 keV, [e] PCA 10-25 keV & [f] PCA 3-25 keV Model Fitted Photon Fluxes in number of $photons/cm^2/s$.

Table 3. Continued.

Obs. (1)	diskbb $T_{in}(keV)$ (2)	diskbb Norm. (3)	Power-Law Index(Γ) (4)	Power-Law Norm. (5)	Black Body Flux[d] (6)	Power-Law Flux[e] (7)	Total Flux[f] (8)	$\chi^2_{red.}$ (9)
128[c]	$1.739^{+0.048}_{-0.059}$	$7.765^{+0.9820}_{-1.0560}$	$1.691^{+0.044}_{-0.047}$	$0.292^{+0.052}_{-0.058}$	$0.2343^{+0.0126}_{-0.0085}$	$0.0433^{+0.0015}_{-0.0012}$	$0.2776^{+0.0142}_{-0.0207}$	1.179
129[a]	$1.253^{+0.021}_{-0.021}$	$24.350^{+2.1200}_{-1.6450}$	$1.859^{+0.016}_{-0.013}$	$0.481^{+0.020}_{-0.013}$	$0.1944^{+0.0006}_{-0.0008}$	$0.0425^{+0.0001}_{-0.0001}$	$0.2369^{+0.0035}_{-0.0029}$	1.140
130[a]	$1.391^{+0.029}_{-0.030}$	$9.544^{+0.8300}_{-0.7620}$	$1.725^{+0.014}_{-0.014}$	$0.332^{+0.013}_{-0.014}$	$0.1542^{+0.0003}_{-0.0007}$	$0.0423^{+0.0001}_{-0.0001}$	$0.1965^{+0.0004}_{-0.0006}$	0.709
131[a]	$1.418^{+0.048}_{-0.054}$	$4.943^{+0.6440}_{-0.6460}$	$1.603^{+0.020}_{-0.021}$	$0.214^{+0.014}_{-0.012}$	$0.1134^{+0.0001}_{-0.0004}$	$0.0379^{+0.0001}_{-0.0001}$	$0.1513^{+0.0003}_{-0.0003}$	0.840
132[b]	$0.735^{+0.048}_{-0.052}$	$43.350^{+7.4300}_{-7.4400}$	$1.604^{+0.028}_{-0.030}$	$0.063^{+0.005}_{-0.005}$	$0.0328^{+0.0008}_{-0.0008}$	$0.0109^{+0.0002}_{-0.0002}$	$0.0438^{+0.0008}_{-0.0010}$	1.075
133[a]	$1.339^{+0.039}_{-0.062}$	$4.379^{+0.7290}_{-0.8320}$	$1.581^{+0.019}_{-0.018}$	$0.173^{+0.010}_{-0.010}$	$0.0906^{+0.0008}_{-0.0007}$	$0.0323^{+0.0001}_{-0.0001}$	$0.1229^{+0.0008}_{-0.0005}$	1.292
134[a]	$1.361^{+0.059}_{-0.067}$	$2.949^{+0.4880}_{-0.5050}$	$1.507^{+0.020}_{-0.021}$	$0.106^{+0.006}_{-0.006}$	$0.0632^{+0.0002}_{-0.0004}$	$0.0242^{+0.0002}_{-0.0002}$	$0.0874^{+0.0008}_{-0.0005}$	1.085
135[a]	$2.049^{+0.085}_{-0.073}$	$0.550^{+0.0440}_{-0.0630}$	$1.213^{+0.049}_{-0.054}$	$0.035^{+0.005}_{-0.005}$	$0.0415^{+0.0008}_{-0.0008}$	$0.0188^{+0.0002}_{-0.0002}$	$0.0603^{+0.0005}_{-0.0005}$	1.546
136[a]	$1.396^{+0.073}_{-0.080}$	$1.463^{+0.3020}_{-0.2730}$	$1.475^{+0.054}_{-0.029}$	$0.055^{+0.006}_{-0.004}$	$0.0349^{+0.0001}_{-0.0003}$	$0.0138^{+0.0002}_{-0.0001}$	$0.0488^{+0.0008}_{-0.0004}$	1.444
137[a]	$1.147^{+0.039}_{-0.015}$	$0.750^{+0.2100}_{-0.3670}$	$1.548^{+0.034}_{-0.036}$	$0.020^{+0.002}_{-0.002}$	$0.0205^{+0.0001}_{-0.0001}$	$0.0041^{+0.0002}_{-0.0002}$	$0.0147^{+0.0004}_{-0.0001}$	1.441
138[a]	$1.404^{+0.022}_{-0.011}$	$1.086^{+0.1890}_{-0.2770}$	$1.479^{+0.045}_{-0.048}$	$0.042^{+0.005}_{-0.005}$	$0.0262^{+0.0010}_{-0.0016}$	$0.0103^{+0.0002}_{-0.0002}$	$0.0364^{+0.0003}_{-0.0006}$	1.003
139[a]	$0.540^{+0.065}_{-0.081}$	$1.230^{+0.1050}_{-0.0890}$	$1.649^{+0.026}_{-0.024}$	$0.019^{+0.003}_{-0.001}$	$0.0081^{+0.0003}_{-0.0005}$	$0.0029^{+0.0002}_{-0.0002}$	$0.0111^{+0.0004}_{-0.0004}$	1.091
140[b]	$0.885^{+0.017}_{-0.017}$	$1.294^{+0.0880}_{-0.0520}$	$1.546^{+0.025}_{-0.023}$	$0.037^{+0.003}_{-0.002}$	$0.0201^{+0.0009}_{-0.0013}$	$0.0076^{+0.0003}_{-0.0002}$	$0.0277^{+0.0002}_{-0.0002}$	0.658
141[a]	$1.119^{+0.018}_{-0.016}$	$1.243^{+0.0670}_{-0.0880}$	$1.603^{+0.035}_{-0.035}$	$0.040^{+0.004}_{-0.004}$	$0.0186^{+0.0001}_{-0.0005}$	$0.0069^{+0.0003}_{-0.0001}$	$0.0256^{+0.0006}_{-0.0006}$	0.683
142[a]	$1.481^{+0.014}_{-0.016}$	$0.284^{+0.0940}_{-0.0840}$	$1.425^{+0.074}_{-0.073}$	$0.011^{+0.003}_{-0.002}$	$0.0077^{+0.0002}_{-0.0002}$	$0.0030^{+0.0001}_{-0.0001}$	$0.0107^{+0.0003}_{-0.0001}$	0.575
143[a]	$1.371^{+0.017}_{-0.014}$	$0.276^{+0.0780}_{-0.0880}$	$1.472^{+0.086}_{-0.088}$	$0.007^{+0.002}_{-0.002}$	$0.0047^{+0.0002}_{-0.0003}$	$0.0017^{+0.0001}_{-0.0001}$	$0.0064^{+0.0004}_{-0.0005}$	0.704
144[a]	$0.455^{+0.013}_{-0.016}$	$0.770^{+0.0700}_{-0.0660}$	$1.761^{+0.011}_{-0.033}$	$0.018^{+0.011}_{-0.013}$	$0.0064^{+0.0004}_{-0.0004}$	$0.0021^{+0.0003}_{-0.0003}$	$0.0085^{+0.0003}_{-0.0004}$	0.854
145[a]	$1.760^{+0.017}_{-0.018}$	$0.118^{+0.0740}_{-0.0700}$	$1.592^{+0.083}_{-0.086}$	$0.020^{+0.005}_{-0.022}$	$0.0103^{+0.0003}_{-0.0005}$	$0.0038^{+0.0007}_{-0.0002}$	$0.0141^{+0.0007}_{-0.0006}$	0.909
146[a]	$0.422^{+0.026}_{-0.021}$	$1.400^{+0.0320}_{-0.0300}$	$1.774^{+0.038}_{-0.037}$	$0.030^{+0.022}_{-0.025}$	$0.0099^{+0.0004}_{-0.0005}$	$0.0033^{+0.0002}_{-0.0003}$	$0.0133^{+0.0006}_{-0.0007}$	0.784
147[a]	$1.931^{+0.055}_{-0.075}$	$0.041^{+0.0200}_{-0.0170}$	$1.771^{+0.014}_{-0.013}$	$0.025^{+0.009}_{-0.009}$	$0.0087^{+0.0013}_{-0.0007}$	$0.0028^{+0.0003}_{-0.0003}$	$0.0115^{+0.0001}_{-0.0007}$	0.799
148[a]	$1.135^{+0.018}_{-0.018}$	$0.713^{+0.1880}_{-0.2070}$	$1.670^{+0.095}_{-0.092}$	$0.015^{+0.004}_{-0.004}$	$0.0067^{+0.0007}_{-0.0007}$	$0.0021^{+0.0001}_{-0.0001}$	$0.0088^{+0.0008}_{-0.0001}$	0.983
149[a]	$1.379^{+0.022}_{-0.023}$	$0.150^{+0.0020}_{-0.1130}$	$1.755^{+0.028}_{-0.027}$	$0.006^{+0.002}_{-0.001}$	$0.0025^{+0.0002}_{-0.0002}$	$0.0027^{+0.0001}_{-0.0001}$	$0.0032^{+0.0002}_{-0.0002}$	0.783
150[a]	$2.455^{+0.036}_{-0.043}$	$0.015^{+0.0020}_{-0.0020}$	$2.300^{+0.024}_{-0.025}$	$0.007^{+0.002}_{-0.001}$	$0.0010^{+0.0001}_{-0.0002}$	$0.0022^{+0.0003}_{-0.0003}$	$0.0012^{+0.0001}_{-0.0002}$	0.687

Fitted with [a]diskbb + power law, [b]diskbb + Gaussian + powerlaw and [c]diskbb + compST + power law

[d]PCA 3-10 keV, [e] PCA 10-25 keV & [f]PCA 3-25 keV Model Fitted Photon Fluxes in number of photons/cm^2/s.

Table 4. F-test results for the 5 set of spectra of Fig.11.

Obs. Id	Set 1*	$\chi^2_{red.}$ & d.o.f.	Set 2*	$\chi^2_{red.}$ & d.o.f.*	F-test Results[†]	Remarks
90704-04-01-00	diskbb + po	4.009, 50	diskbb + compST + po	2.582, 47	8.690, 1.078e-04	
90704-04-01-00	diskbb + po	4.009, 50	diskbb + ga + po	1.019, 48	70.438, 5.266e-15	Set 2 was used
91702-01-02-00G	diskbb + po	2.121, 50	diskbb + compST + po	1.085, 47	14.957, 5.723e-07	
91702-01-02-00G	diskbb + po	2.121, 50	diskbb + ga + po	0.875, 48	34.166, 5.928e-10	Set 2 was used
91702-01-08-00	diskbb + po	3.621, 45	diskbb + compST + po	2.716, 33	0.916, 0.542	
91702-01-08-00	diskbb + po	3.621, 45	diskbb + ga + po	2.210, 43	10.043, 2.636e-04	Set 2 was used
91702-01-57-00G	diskbb + po	2.778, 50	diskbb + compST + po	0.936, 47	30.811, 3.644e-11	
91702-01-57-00G	diskbb + po	2.778, 50	diskbb + ga + po	0.934, 48	49.804, 1.955e-12	Set 2 was used
91702-01-79-00	diskbb + po	8.172, 50	diskbb + compST + po	1.179, 47	92.924, 8.981e-20	
91702-01-79-00	diskbb + po	8.172, 50	diskbb + ga + po	4.99, 49	51.358, 3.665e-09	Set 2 was used

*diskbb: disk black body, po: power-law, ga: Gaussian, compST: Sunyaev & Titarchuk Comptonization model, d.o.f.: Degrees of Freedom.

[†]F-test was done between Set 1 and Set 2 model fitted results and in the column F statistic value & probability values were given.

Table 5
Fitted data with two component flow model

Date	MJD	Halo rate	Disk rate
Mar. 3, 2005	53432.7930	0.015	0.0100
Mar. 9, 2005	53438.0539	0.004	0.0400
Mar. 10, 2005	53439.7400	0.009	0.0650
Mar. 11, 2005	53440.6780	0.0043	0.5100
Mar. 12, 2005	53441.5109	0.0100	0.7800
May 16, 2005	53506.9531	0.0550	1.5640
May 20, 2005	53510.0994	0.0560	1.7400
Sep. 16, 2005	53629.3761	0.0038	0.0700
Sep. 19, 2005	53632.4557	0.0029	0.0300
Sep. 22, 2005	53635.4696	0.0065	0.0140
Sep. 29, 2005	53641.0383	0.009	0.0100

and as a result the total flux could be almost constant. In outburst sources, on the other hand, the approaching and receding Keplerian component in the rising and decline phases causes the net flux to rise and fall during the hard to soft and intermediate to hard state respectively.

4.   Concluding remarks

In this paper, we presented a comprehensive analysis of the entire 2005 outburst of GRO J1655-40. The results clearly indicated that the spectral state passed from the hard state in the onset phase with a poor Keplerian component to the soft/very soft and intermediate states dominated by Keplerian disks and finally to the hard state at the decline phase. It is often believed that low frequency QPOs may be generated by perturbations at the inner edge of a Keplerian disk, either by orbiting 'blobs' or more probably oscillating shocks. Our observation of the smooth variation of the QPO frequency during the onset and the decline phases indicates that whatever be the reason for QPO, it has to survive for weeks. It is difficult to imagine that disk perturbation with blobs be sustained for such a long time without being sheared and dissipated. On the other hand, shock oscillations have been shown to survive for a long period and the PDS calculated from observations also resembles the observed PDS. QPO frequencies at the onset and decline phases have been shown separately (Chakrabarti et al. 2005, 2008, 2009) to be simply related as though an oscillating shock is drifting in at the rising phase and drifting out at the decline phase. We therefore favour the shock oscillation solution of the low and intermediate frequency QPOs. Recently (Titarchuk, Shaposnikov & Arefiev 2007) have pointed out that the presence of bumps in the PDS of Cyg X-1 is the signature of a sub-Keplerian flow in the accretion disk. We have also observed similar bumps on days which have significant halo component (see, Fig. 4c and Table 5). Thus we believe that the general picture which emerged out of our analysis is consistent with a two component advective flow as has been pointed out by many authors in the context of several black holes (Smith et al. 2001; Smith, Heindl & Swank 2002; Smith, Dawson & Swank 2007). The TCAF model is further supported by a clear indication of a jump in total flux at the state transitions (hard to soft and intermediate to hard) in this source. This we believe is due to the approaching and receding Keplerian component in the rising and declining phases.
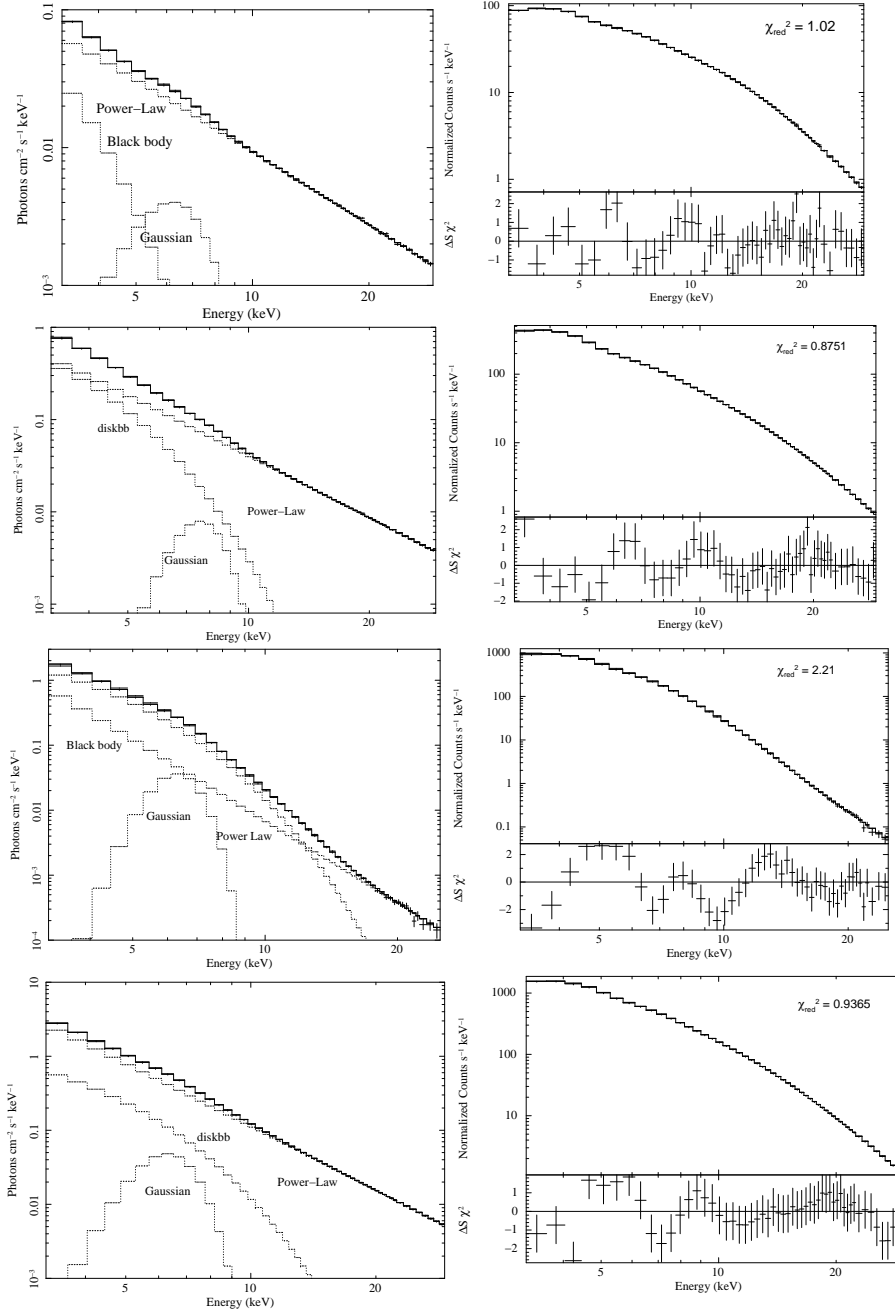
Fig. 11(a-d): 3-25 keV RXTE/PCA model fitted spectra with various components on the left panels and the fitted reduced χ^2_{red} on the right panels. Data used are of (a) 10th March, 2005 (Obs ID: 90704-04-01-00), (b) 11th March, 2005 (ID: 91702-01-02-00G), (c) 20th March, 2005 (ID: 91702-01-08-00), (d) 17th May, 2005 (ID: 91702-01-57-00G) respectively.
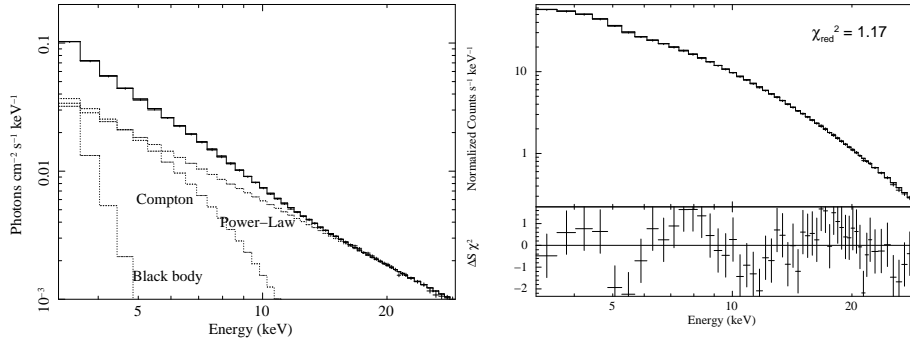
Fig. 11(e): Same as Fig. 11(a-d) except the data of 17th September, 2005 (ID: 91702-01-79-00) was used.

This is in contrast with persistence X-ray sources, such as Cyg X-1, where the total flux remains constant.

Acknowledgments

References

Bailyn, C. D., Orosz, J. A., McClintock, J. E. & Remillard, R. A., 1995, Nature, 378, 157

Brocksopp, C. et al. 2006, MNRAS, 365, 1203

Chakrabarti, S.K., Acharyya, K. & Molteni, D., 2004, 421, 1

Chakrabarti, S.K., Datta, B.G. & Pal, P.S., 2009, MNRAS (in press)

Chakrabarti, S.K., Debnath, D., Nandi, A. & Pal, P.S., 2008, A& A, 489, L41

Chakrabarti, S.K. & Mandal, S. 2006, ApJ, 642, 49

Chakrabarti, S.K. & Manickam, S. 2000, ApJ, 531, 41

Chakrabarti,S.K., Nandi, A., Debnath, D., Sarkar, R. & Datta, B.G., 2005, IJP 79(8), 841

Chakrabarti, S. K. & Titarchuk, L. G., 1995, ApJ, 455, 623

Chen, W., Shrader, C. R. & Livio, M. 1995, APJ, 454, 880

Daz Trigo, M., Parmar, A. N., Miller, J., Kuulkers, E. & Caballero-Garca, M. D. 2007, A& A, 462, 657

Ebisawa, K., Titarchuk, L.G. & Chakrabarti, S.K., 1996, PASJ, 48, 59

Foellmi, C., Depagni, P., Dall, T.S. & Mirabel, I.F. 2006, A & A, 457, 249

Hjellming, R. M. & Rupen, M.P., 1995, Nature, 375, 464

Jahoda, K., 1996, Proc. SPIE, 2808, 59

Levine, A. M., et al., 1996, APJ, 469 L33

Markwardt, C. B. & Swank, J. H. 2005, ATel, 14, I

Molteni, D., Sponholz, H. & Chakrabarti, S. K., 1996, ApJ, 457, 805

Nowak, M. A., 2000, MNRAS, 318, 361

Orosz, J.A., & Bailen, C.D., 1997, ApJ 477, 876

Papadakis, I. E., Lawrence, A 1993, MNRAS, 261, 612

Remillard, R.A. et al. 1999, ApJ, 552, 397

Ryu, D., Chakrabarti, S. K. & Molteni, D., 1997, ApJ, 474, 378

Shaposhnikov, N. et al. 2007, ApJ, 655, 434

Saito, K., et al., 2006, in POS, Proceedings of VIth Microquasar Workshop: Microquasars & Beyond, 93

Smith, D., Heindl, W. A. & Swank, J. H., 2002, ApJ, 569, 362

Smith, D.M., Heindl, W.A., Markwardt, C.B. & Swank, J.H., 2001, ApJ, 554, L41

Smith, D.M., Dawson, D. M. & Swank, J. H., 2007, ApJ, 669, 1138

Sobczak, G.J. et al. 1999, ApJ, 520, 776

Soria, R., Wu, K., Hannikainen, D., McMollough, M. & Hunstead., R., 2001,

Strohmayer, T. E., 2001, ApJ, 552, 49

Takahashi, H. et al. 2008, PASJ, 60, 69

Tingay, S.J., et al., 1995, Nature, 374, 141

Titarchuk, L.G., Shaposhnikov, N. & Arefiev, V., 2007, ApJ, 660, 556

Trudolyubov S., Churazov E. & Gilfanov M., 1999, A&A, 351, 15

van der Klis, M. 2005, AN, 326, 798

Vignarca, F., Migliari, S., Belloni, T., Psaltis, D. & van der Klis, M. 0., 2003, A & A, 397, 729

Wu, K. et al., 2002, ApJ 565, 1161

Zhang, S.N., et al. IAU Circ., 1994, 6046

Zhang, S.N. et al. 1996, ApJ 477, L95